“RH1”

2021-2022 AIAA DBF Competition

University of Massachusetts Lowell

Table of Contents

AIAA	American Institute of Aeronautics and Astronautics
DBF	Design Build Fly
M1	Mission 1 Score
M2	Mission 2 Score
M3	Mission 3 Score
GM	Ground Mission Score
W/P	Weight to Power
W/S	Wing Loading
L	Lift
D	Drag
$C_{l,max}$	Maximum section lift coefficient
$C_{d,min}$	Minimum section drag coefficient
V_{stall}	Stall speed
V_{max}	Maximum speed
L_{TO}	Take off length
S	Wing planform area
AR	Aspect ratio
b	Wingspan
c	Chord
C_L	Lift coefficient
C_D	Drag coefficient
$C_{m_{o\ w}}$	Wing moment coefficient
h	Normalized distance from wing leading edge to center of gravity
h_0	Normalized distance from wing leading edge to aerodynamic center
l	Tail arm
η_H	Horizontal tail efficiency
$\bar{V}_H$	Horizontal tail volume
S_H	Horizontal tail planform area
C_{L_H}	Horizontal tail lift coefficient
$\bar{V}_V$	Vertical tail volume
CG	Center of gravity
LiPo	Lithium Polymer
NiMH	Nickel–metal hydride
CFD	Computational Fluid Dynamics
C_{D_P}	Parasite drag coefficient
K	Form factor
C_f	Skin friction coefficient
S_{wet}	Wetted area
S_{ref}	Reference area
CAD	Computer aided design
ω_n	Undamped natural frequency
ω_d	Damped natural frequency
ζ	Damping ratio
τ	Time constant
V_{cruise}	Cruise speed
ESC	Electric speed control
EHS	Environmental Health & Safety
ACM	Assembly Crew Member
TOGW	Takeoff Gross Weight
$C_{L_{max}}$	Maximum lift coefficient
$C_{L_{cruise}}$	Cruise lift coefficient

1.0 Executive Summary

The following report outlines the design, manufacturing, and testing of the University of Massachusetts Lowell's (UML's) entry into the 2021-22 American Institute of Aeronautics and Astronautics (AIAA) Design, Build, Fly (DBF) competition. The model of the RH1 aircraft is depicted in Figure 1.

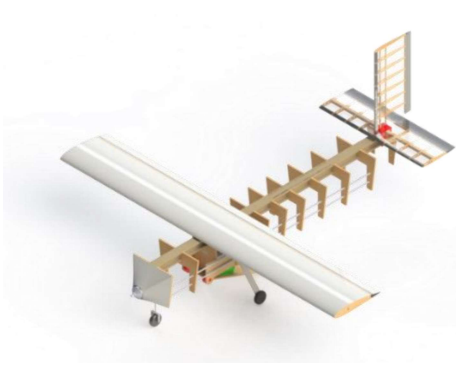

Figure 1. Model of the RH1 aircraft

The objective for the aircraft as designated by the AIAA DBF organizing committee is outlined below:

Mission 1 – Deployment Flight: The aircraft must take-off in 25 feet or less, and complete 3 laps within a 5-minute period. A successful landing is required to complete this mission. No payload will be present for this flight. Below shows the layout of the course.

Mission 2 – Staging Flight: The aircraft must complete the same task as mission 1; a payload of at least 10 syringes must be carried. A successful landing is required to complete this mission

Mission 3 – Vaccine Delivery Flight: The payload for Mission 3 is vaccine vial packages. The aircraft must fly the standard mission profile as shown above for each lap. The aircraft then can land on the runway and taxi to a designated package drop area and remotely deploy one vaccine vile package. After successful deployment the aircraft can taxi back to the starting line and run the flight again until every vaccine vile package is deployed.

Ground Mission – Timed, ground demonstration of loading payloads for Missions 2 and 3.

A scoring analysis and deliberation of the airfield location was conducted throughout the preliminary design phase and concluded that 10 syringes for Mission 2 and 1 vaccine vile package for Mission 3 would be the optimal payload configuration without compromising score.

In the conceptual design phase, the team decided on a high-wing, single propellor aircraft. The fuselage was designed with an emphasis on ease of assembly to not interfere with the integration of other components of the aircraft.

2.0 Management Summary

The University of Massachusetts Lowell (UML) AIAA-DBF team is comprised of both upperclassmen and underclassmen. The team's faculty advisors provide guidance as well as an interface between the team and the Mechanical Engineering Department. The student team is comprised of mechanical engineering undergraduates that have adopted a shared leadership structure, with students arranged in sub-teams. Underclassmen are encouraged to continue this project as a senior-level capstone or as a directed study for course credit, both of which are led by the same faculty advisors.

2.1 Team Structure

The team is divided into five primary sub teams as presented in figure 2.1.

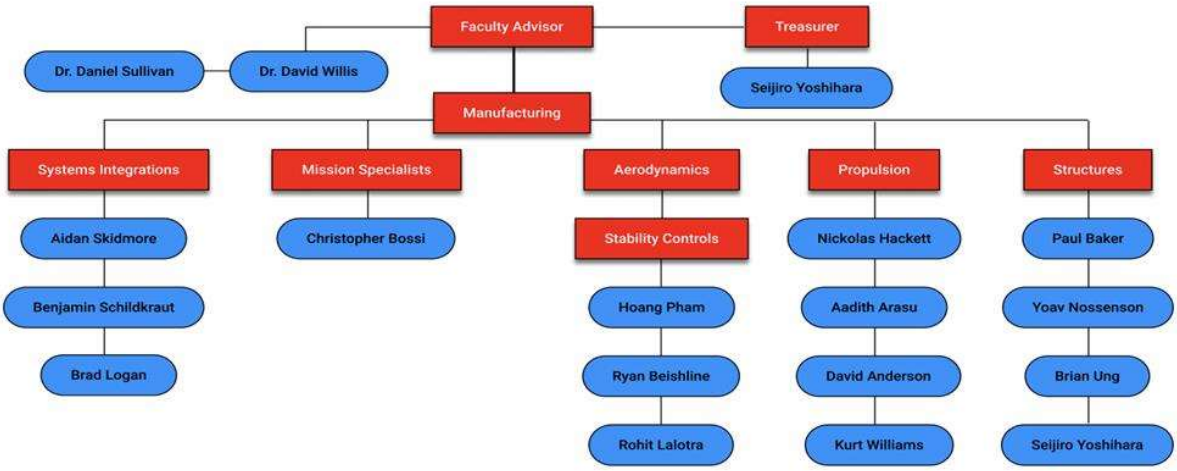

Figure 2.1: Team Organization chart featuring sub teams and sub team members

The specific sub teams were tasked with the responsibilities as shown in the table below

Table 2.1: Sub teams and their responsibilities for the creation of the aircraft

Sub teams	Responsibilities
Advisors	Monitor Progress, and Interact with Administration
Treasurer	Responsible for securing funding and budgeting/purchasing parts
Systems Integration	Design CAD models and inspect weights to ensure a balanced aircraft
Mission Specialists	Examine missions and competition rules to increase the efficiency of scoring points
Aerodynamics	Design the outer shape of the aircraft through aerodynamic theory and computation
Propulsion	Conduct tests and calculations to find suitable motors, batteries, and ESC

Structures	Perform test and simulations to design the load-bearing structure of the aircraft
Manufacturing	Develop the manufacturing approach while considering various build techniques and safety
Stability Controls	Conduct static and dynamic stability analysis and size the control surfaces

2.2 Milestone Chart

To better strategize the development of the aircraft, the team created a Gantt chart as shown below in Figure 2.2. The chart was based on the milestones present in the 2021-2022 DBF competition and what tasks needed to be completed to meet those milestones.

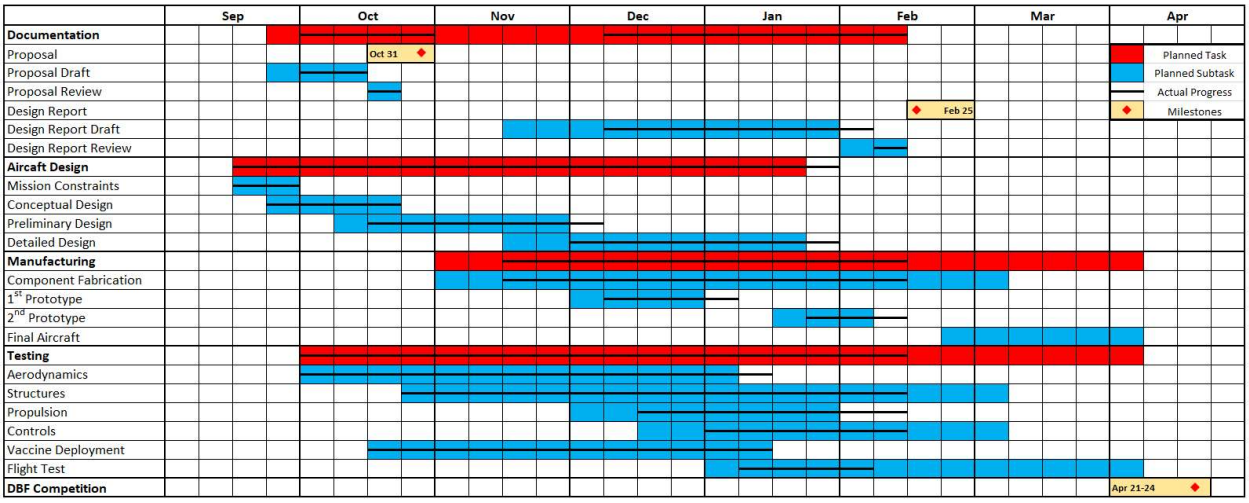

Figure 2.2: UML AIAA-DBF Team Gantt chart for the 2021-22 competition

The creation of the Gantt chart served as a valuable resource for the team as it acted as a method to ensure that the project would continue at a reasonable pace. The Gantt chart served to prioritize the team's objectives and meet key milestones.

3 CONCEPTUAL DESIGN

At the conceptual design stage, care will be taken to review the general requirements, mission requirements, and scoring analysis were considered to determine a strategy that can be translated into design requirements.

3.1 General Requirements

This section outlines the requirements which apply to the competition aircraft in all four missions.

3.1.1 Aircraft Requirements

1. The maximum linear dimension of the aircraft must not exceed 8ft.

2. Rotary wing and lighter-than-air aircraft are forbidden.
3. The maximum takeoff gross weight (TOGW) is 55lbs.
4. The aircraft's battery capacity must not exceed 100 W-h.

3.2 Mission Requirements

This section will review the requirements and scoring criteria specific to each of the four missions in this year's competition.

3.2.1 Mission 1 – Deployment Flight

In the 2021 – 2022 DBF Competition Rules mission 1 (M1) has been labeled the deployment mission and will serve to test the aircraft's airworthiness. The aircraft must take-off in 25 feet or less, and complete 3 laps within a 5-minute period. A successful landing is required to complete this mission. No payload will be present for this flight. M1 scoring is listed below:

$$M_1 = 1.0\ (sucessful\ completion)$$

3.2.2 Mission 2 – Staging Flight

Mission 2 (M2) will test the aircraft's ability to deliver supplies (syringes) needed to administer vaccines. The mission duration, takeoff distance, and number of laps are the same as M1, 5 minutes, 25ft or less, and 3 laps, respectively. A payload of at least 10 syringes must be carried. A successful landing is required to complete this mission. M2 scoring is listed below:

$$M_2 = 1 + \frac{\#syringe/time_{UML}}{\#syringe/time_{MAX}}$$

3.2.3 Mission 3 – Vaccine Delivery Flight

Mission 3 (M3) will assess the ability of the aircraft to deliver undamaged vaccine vial packages. The payload for this mission will be simulated vaccine vial packages. These packages will be constructed using a 2.5" x 3.0" x 3.5" wooden block with 25G shock sensors on each longitudinal axis. Takeoff distance is the same as M1 and M2, 25ft or less. The mission maximum duration is 10 minutes. The number of laps will correspond to the number of vial packages carried as one package must be delivered per lap. Additionally, the maximum number of packages that can be carried will be limited to the number of syringes carried in M2 divided by 10. After each successful lap the aircraft must land and deploy a vaccine vial package. A successful deployment is defined as package being delivered to specified area, 25ft prior to the start line, and no tripped shock sensors. A successful landing is required to complete this mission. Scoring is based on each successfully deployed package. The scoring equation is below:

$$M_3 = 2 + \frac{\#succesful\ deployments_{UML}}{\#succesful\ deployments_{MAX}}$$

3.2.4 Ground Mission – Operational Demonstration

The ground mission (GM) is designed as a proof of concept for the aircraft systems in a controlled environment. The mission starts with the aircraft, the uninstalled number of vial packages declared in tech inspection and the corresponding to the number of syringes, 10 times the number of vial packages, in the "mission box" (a 10ft square area). The pilot and assembly crew member (ACM) will be standing outside of the mission box. Only the assembly crew members can touch the aircraft. When the official says, "GO" timer will start, the ACM will enter the mission box, load the syringes then exit the mission box as quickly as possible – timer will stop. When the official says, "GO" again, the timer will restart, the ACM will reenter the mission box remove the M2 payload then load the M3 payload and exit the mission box – the timer will stop. The pilot will then deploy all the packages. All packages must be successfully deployed to successfully complete the mission. Scoring is based on your team's total GM time compared to the fastest team competing. Scoring equation is below:

$$GM = \frac{time_{MIN}}{time_{UML}}$$

3.2.5 Total Score

The total competition score is based on the total mission score multiplied by the design report score. The calculations are reflected below.

$$Total\ Mission\ Score = M_1 + M_2 + M_3 + GM$$

$$SCORE = Design\ Report\ Score * Total\ Mission\ Score$$

3.3 Scoring Analysis

The scoring analysis helped identify which aircraft characteristics would take priority in the conceptual design. After reviewing the rules, 3 key independent variables were selected to be manipulated to study their effects on the final score. The variables are as follows:

- **Number of Vial Packages** – Based on the rules this value would be dependent on the number of syringes carried. However, for this analysis the decision was made to view this relationship in the reverse and base the number of syringes on the number of vial packages carried. This simplifies the analysis as it decreases the number of independent variables to be considered. This view is also in line with our team's process of choosing the number of packages to deliver and working backwards. Additionally, a value of 60 seconds per vial package was used to calculate the ground mission duration. The assumption for other teams' maximum number of vial packages was set at 8, based on the idea that at the average maximum velocity, of the top three finishers from previous 3 competitions, only about 8 laps/deployments could be successfully completed in a 10-

minute period. The nominal value for the analysis was set at four as it provided a good median value.

- **Time of Mission 2** - the denominator of the mission's unnormalized score. A nominal value of 171 seconds was used as it allowed for a +/-75% variation without exceeding the 5 minutes allotted or crossing too far beyond the maximum possible speeds for these craft. The assumption used to calculate the # of syringes/time variable was 120 seconds thus yielding the value in Table 3.1.
- **Report Score** - the base multiplier for the final score. The nominal value was based on the 10-year average of UML DBF Score.

Mission Variable Assumptions	
Variable	**Value**
Maximum # of Syringes/Time Value	0.66
GM Lowest Time (sec)	60

Table 3.1: Mission Variable Assumptions for Scoring Analysis

Table 3.2: Nominal Values for Independent Variables for Scoring Analysis

Nominal Values for Independent Variables	
Variable	**Value**
Number of Vial Packages	4
Mission 2 Time (sec)	171
Report Score	80

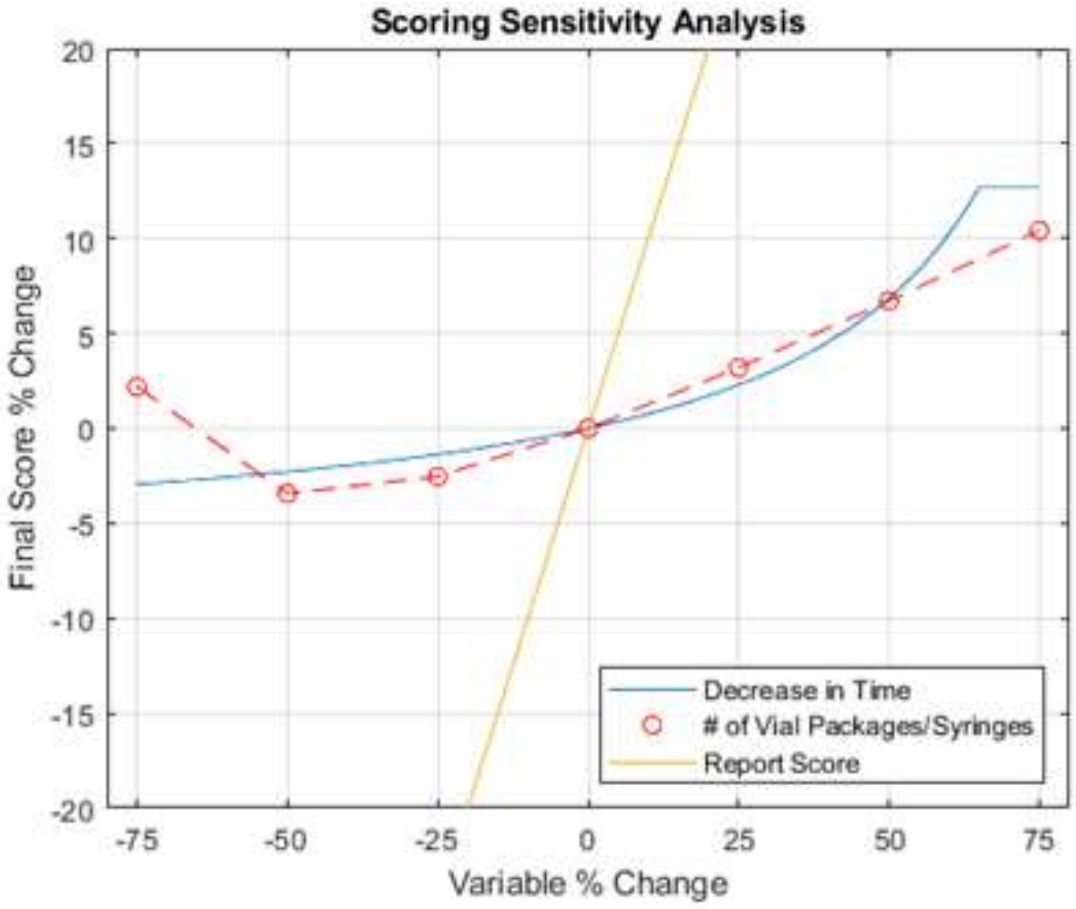

***F**igure 3.1: Scoring Sensitivity Analysis*

The scoring analysis presented an interesting insight. Based on the linear relationship that was established between the number of vial packages and the ground mission time. It would be necessary to carry 5 or more vial packages to make up for the points lost on the longer ground

mission. Trying to decrease the M2 time beyond 50% would be challenging, based on historical data, and not would not make much of a difference if only 10 syringes are carried. A good solution to maximize the mission 2 score with a lesser syringe payload was to aim for 30 syringes and decrease the time by 30%. Furthermore, by choosing to fly only 1 lap in mission the exposure to the high wind conditions traditionally present at the Wichita Kansas airfield can be decreased.

3.4 Analysis Based Design Requirements

After considering the general requirements, mission requirements, and scoring analysis some key design requirements have been established:

- **High Thrust to Weight Ratio** – The requirement of a 25ft takeoff necessitates an aircraft that can quickly achieve enough velocity to take off. Additionally, high thrust is needed to minimize lap time.
- **Precise Deployment System** – The 25G sensor is very sensitive and any inaccuracies from the mechanism could cause the sensor to trip.
- **Short Payload Load Time** – developing a system that will minimize load time is essential to a good score in the ground mission.
- **Strong and Compliant Landing Gear** – Concern about the 25G sensor tripping while landing or taxing can be addressed with the right landing gear design.

3.5 Configuration Selection

3.5.1 Wing

Table 3.3: Wing placement considerations

Wing Configuration		Low Wing	Mid Wing	High Wing
Categories	Weight [1-5]	Value [1-10]	Value [1-10]	Value [1-10]
Stability	5	5	6	8
Structural Strength	4	8	6	9
Manufacturability	4	7	6	7
Cargo Space	3	7	5	8
Total		106	93	**128**

For the wing configuration, the stability of the aircraft was the most important criteria to ensure that the aircraft can safely fly through disturbances during flight (tailwind, headwind, crosswind, etc.). The structural strength is also a key design criterion since the wing will have to withstand different distributed forces during each mission. In addition, the manufacturability of the wing and the attachment method also play an important role in deciding the wing configuration. Finally, the wing configuration also affects the amount of cargo space, which is pivotal for the transportation of the syringes in mission 2. As a result, a decision matrix, shown in Table 3.3, was used to pick the best option. From Table 3.3, the high wing is

the best configuration based on the criteria. The high wing has an increase in dihedral effect; therefore, the aircraft will be more stable laterally. Additionally, for the high wing configuration, the whole wing can be supported by a single beam that crosses the fuselage (instead of cantilever beams for the mid wing configuration), so the wing will not fail due to the large bending moments at the attachment point. On top of that, the high wing will only require one mounting point on the top of the fuselage, so it is slightly simpler to manufacture and integrate, and there will be more room in the fuselage for the payload. Hence, the high wing configuration was chosen for the aircraft.

Table 3.4: Wing planform Decision Matrix

Wing Planform		**Rectangular**	**Tapered**	**Elliptical**
Categories	Weight [1-5]	Value [1-10]	Value [1-10]	Value [1-10]
Aerodynamics	3	6	8	10
Controllability	4	8	7	6
Structural Strength	4	7	8	4
Manufacturability	5	9	7	6
Total		**123**	119	100

With the configuration determined, the planform (or shape) of the wing was subsequently selected. The wing is responsible for generating much of the lift for the aircraft; therefore, aerodynamics was one of the criteria of the planform. Furthermore, the implementation of the control surfaces, which is important for the controllability of the aircraft, and the structural strength also had a crucial role in deciding the planform. Finally, the most important parameter for the planform was the manufacturability. Table 3.5 shows the decision matrix to weigh the different planform options, and the rectangular was the optimal choice. The rectangular platform had disadvantages such as an undesirable lift distribution [4] compared to the tapered and elliptical configuration, and its strength to weight ratio was slightly lower than the tapered configuration. However, it was the best option for the manufacturability of both the wing and control surfaces. Additionally, since the integration of the control surfaces is more reliable for the rectangular planform, the aircraft would also be more controllable. In turn, the rectangular planform was the best option for the aircraft.

3.5.2 Tail

Table 3.5: Tail Configuration Decision Matrix

Tail Configuration		Conventional	T-Tail	H-Tail
Categories	Weight [1-5]	Value [1-10]	Value [1-10]	Value [1-10]
Stability & Control	5	9	8	6
Structural Strength	5	7	6	5
Manufacturability	3	8	7	5
Efficiency	2	5	8	9
Total		**114**	107	88

The stability and control of the aircraft had the most significant influence on the tail configuration decision since the main function of the tail is to control the aircraft during takeoff, landing, and turning and to keep the aircraft stable during cruise. Because of this, the structural strength of the tail is also pivotal to ensure that failure does not occur during these critical operations. The manufacturability was also an important consideration for the tail configuration. Finally, efficiency, which indicates how well the tail operates when there is a wake from the wing or fuselage [3], was also compared. Table 3.5 shows the decision matrix to compare the different tail configurations, and the conventional tail was the most ideal configuration. On one hand, the conventional tail would likely be affected by the wake of the wing; however, if the aircraft was designed to not exceed a certain angle of attack, this would not be an issue. On the other hand, the configuration was superior in terms of stability & control, structural strength, and manufacturability. Since only one elevator and one rudder had to be employed for the tail, the aircraft would be easier to control compared to the two rudders of the H-Tail configuration. Besides that, the load of the conventional tail can be directly transferred to the fuselage, so the tail has a better strength to weight ratio compared to the T-Tail (which require extra structural weight from the bending moment from the horizontal tail) and H-Tail configuration (which require extra structural weight to support the vertical tails). Additionally, the conventional tail was also easier to fabricate and mount. As a result, the conventional tail was employed for the aircraft.

3.5.3 Propulsion

To select propulsion components, a decision matrix was created to find the balance between performance, logistics, and simplistic design. The decision matrix as shown in Table 3.6, takes into consideration the amount of knowledge, manufacturability, cost, and efficiency into account and each configuration is given a value ranging from 1 - 10, 1 being the least favorable and 10 being the most favorable.

Table 3.6: Propellor Decision Matrix

Propeller Configuration	Puller (Single Motor)	Pusher (Single Motor)	Twin Propeller (Double Motor)

Categories	Weight [1-5]	Value [1-10]	Value [1-10]	Value [1-10]
Manufacturability	4	10	10	6
Efficiency	4	9	7	10
Knowledge	3	10	8	5
Cost	4	9	9	2
Total		**142**	128	87

As seen in Table 3.6 the most efficient design would be the single motor puller configuration due to cost efficiency, with proven performance efficiency and knowledge from past years.

3.5.4 Landing Gear Configuration

Table 3.7: Landing Gear Decision Matrix

Landing Gear Configuration		Tricycle	Tail dragger	Quadricycle
Categories	Weight [1-5]	Value [1-10]	Value [1-10]	Value [1-10]
Compliance	5	9	6	7
Structural Strength	5	8	5	6
Manufacturability	4	7	8	7
Ground Clearance	5	9	4	3
Total		**158**	107	108

Based on the decision matrix in Table 3.7, a tricycle gear would be the choice for the landing gear configuration. Considering the need for ground clearance on a single prop aircraft and the need to deploy the box from the bottom all while allowing for a soft landing the tricycle gear will be a good fit for the aircraft design.

3.5.5 Syringe Storage

Table 3.8: Syringe Storage Decision Matrix

Syringe Storage		Bag	Box	Caddy
Categories	Weight [1-5]	Value [1-10]	Value [1-10]	Value [1-10]
Speed of Fill	5	9	8	4
Mounting	4	9	6	5
Manufacturability	4	7	8	7
Weight	3	9	6	7
Total		**136**	114	89

The syringe storage is key to speed of the ground mission but must also keep the syringes secure. The box would be almost as fast as the bag but due to the non-cylindrical shape of the bottom of the syringes they can stack a bit odd in a cuboid vessel. The caddy would be great for organizing but loading the syringes into it would be time-consuming.

3.5.6 Deployment Mechanism

Based on the decision of carrying only a single Vaccine Vial Package, a deployment mechanism design needed to be selected. The main factors governing the selection of deployment mechanism design were

complexity of the system, the amount of space the system would require, the manufacturability, and the integration time of the vial packages. The following system designs were compared, and down selected as shown in Table 3.9.

- Ramp: Simple design with quick integration time wherein the vaccine vial package is held in place by a large door that would then, upon deployment, function as a ramp for the box to be slid down to the ground.
- Lowering System: System wherein the vaccine vial package would be lowered to the ground via a winch system. This design required little internal volume compared to its alternatives.
- Suspension Drop System: By controlling the height of the landing gear, the fuselage of the aircraft could be lowered to the ground such that the box could be placed on the ground.

Table 3.9: Deployment Mechanism Decision Matrix

Deployment Mechanism Configuration		**Ramp**	**Lowering system**	**Suspension Drop System**
Categories	Weight [1-5]	Value [1-10]	Value [1-10]	Value [1-10]
Complexity	5	8	6	3
Size	2	6	8	5
Manufacturability	3	8	5	4
Payload integration	4	9	4	9
Total		**112**	77	73

As shown in Table 3.9, the Ramp design was selected due to its rapid payload integration time as well as its simple design.

4.0 Preliminary Design

4.1 Design methodology / analysis methodology

The preliminary design stage started with defining all the constraints (such as the maximum take-off length and the field altitude) and the targeted specifications (such as stall speed or rate of climb) for the aircraft. From there, a weight to power (W/P) vs wing loading (W/S) plot was constructed to find an acceptable region for the parameters, and an initial design point was chosen to maximize the wing loading while maintaining a high W/P. The scoring analysis was also developed during this time to select an appropriate number of syringes and vaccine vial packages for the missions, which resulted in an estimation for the maximum takeoff weight of the aircraft. With the weight and wing loading decided, the initial airfoil was chosen, the initial wing sizing was conducted, and the propulsion system was selected. The control surfaces and empennage were designed iteratively to meet the takeoff and flight stability requirements. The fuselage was developed simultaneously to accommodate the payload and the tail arm. Mission models were also developed to simulate the aircraft performance for each mission. Several iterations were tested to improve the score until a certain threshold was achieved.

4.2 Design and Sizing Trades

4.2.1 Airfoil Selection

From the initial weight estimation, a $C_{l,max} = 1.3$ was required for the aircraft to perform the takeoff and landing safely with a low stall speed of 35 ft/s. Multiple airfoils such as the E332, NACA 2415, and the GOE 628 were selected for consideration based on the $C_{l,max}$ criteria, and their drag polar, thickness, manufacturability were compared to determine the best option for the aircraft. The airfoils were analyzed in XFOIL at a Reynolds number of 500,000 to simulate cruise conditions. As seen in Figure 4.1, all three airfoils satisfy the maximum section lift coefficient requirement. However, the E332 airfoil only has a $C_{l,max} = 1.33$, which is only marginally (2%) higher than the requirement. Furthermore, the E332 airfoil has a lower stall angle of $11.3°$ compared to the remaining two airfoils, and the airfoil's minimum drag coefficient is like the NACA 2415 airfoil. As a result, based on the analysis results, the E332 airfoil was not picked because it did not perform as well as the other airfoils.

The NACA 2415 and GOE 628 airfoil was subsequently compared to determine the optimal choice. The two airfoils have similar smooth stall characteristics and stall angles, with the GOE 628 airfoil having a slightly $1°$ higher stall angle. As seen in Figure 4.1, the GOE 628 airfoil produces more lift overall, reaching a $C_{l,max}$ of 1.73. These characteristics made the GOE 628 airfoil a better option initially; however, further considerations proved otherwise. As seen in Figure 4.1, the GOE 628 airfoil has a 33% higher $C_{d,min}$ compared to the NACA 2415 airfoil, and it produces more drag overall, which will result in more power required for the propulsion system during flight. Furthermore, the GOE 628 airfoil has a higher thickness overall (with a maximum of 17%) compared to the 15% thickness of the NACA 2415 airfoil. In turn, if the GOE 628 airfoil were picked, the wing would weigh more. On top of that, the GOE 628 airfoil also has more camber than the NACA 2415, especially near the trailing edge. This would increase the difficulty of manufacturing the airfoil itself and the control surfaces for the wing.

As a result, NACA 2415 was chosen as the airfoil for the wing based on the reasonable lift coefficient and stall angle, the low minimum drag coefficient, the weight benefits, and the manufacturability.

For the vertical tail, a symmetrical airfoil must be chosen to ensure symmetrical yaw control during cruise. For the horizontal tail, a symmetrical airfoil is also usually chosen for better control. As a result, the NACA 0009 airfoil for the empennage because of its symmetry and its low thickness, which would result in less weight in the aft section of the aircraft.

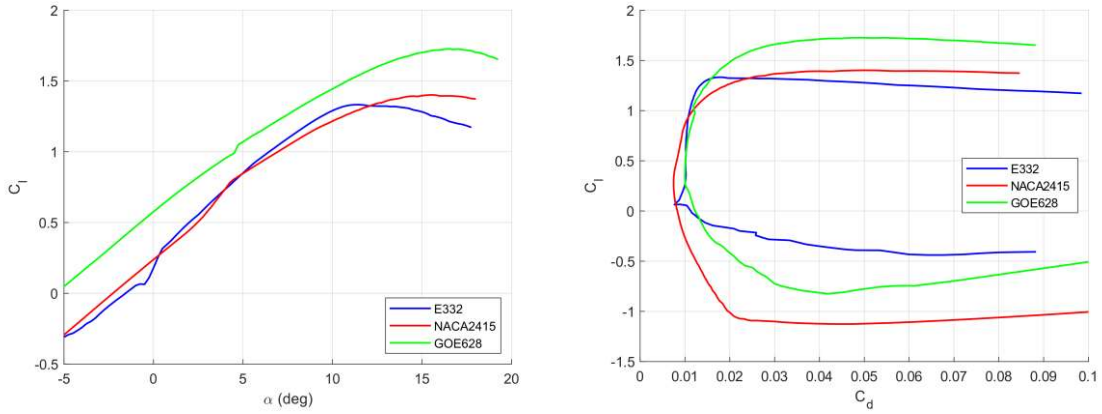

Figure 4.1 - Lift coefficient vs angle of attack (left) and the drag polar (right) of the airfoils

Table 4.1 - Aerodynamic characteristics of airfoils

$\boldsymbol{Airfoil}$	$\boldsymbol{C_{l,max}}$	$\boldsymbol{C_{d,min}}$	$\boldsymbol{Stall\ Angle\ (deg)}$
E332	1.33	0.0076	11.3
NACA 2415	1.40	0.0075	15.5
GOE 628	1.73	0.0100	16.5

4.2.2 Wing Sizing

With the constraints defined early in the stage of the design, the weight to power was calculated as a function of the wing loading depending on different variables [1]: stall speed, maximum speed, takeoff length, rate of climb, and maximum altitude. This resulted in a weight to power vs wing loading curves shown in 4.2 which was used to determine an acceptable region for the parameters and to choose an initial design point.

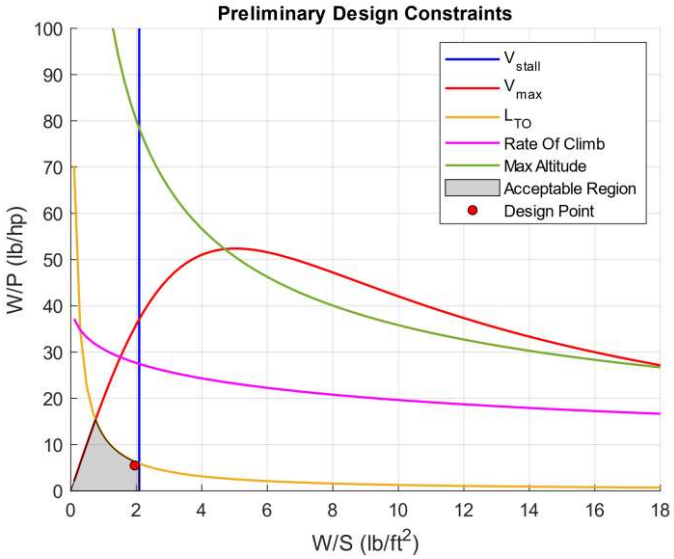

Figure 4.2: Preliminary Design Constraints

As seen in Figure 4.2, the stall velocity, the maximum velocity, and the takeoff length are prime factors that affected the initial sizing of the wing.

To maximize the wing loading while maintaining a low weight to power factor, the wing loading was determined to be 2 lb./ft2. With the historical data of previous aircraft and an approximated weight for the components of the hardware and payload, the maximum take of weight of the aircraft was estimated to be 7.24 lbs. This resulted in a planform area S = 3.62 ft2 required for the wing. With the wing area decided, the taper ratio, aspect ratio, and setting angle.

For ease of manufacturing of the spar, the ribs, the leading edge, and the control surfaces, a rectangular wing was chosen for the aircraft. From there, a study was conducted to study the aerodynamic effects of the aspect ratio using XFLR5 and to choose the optimal option. As seen in Figure 4.3, as the AR increases, the ratio of lift to drag increases. However, at the higher aspect ratios of 7 or 8, the C_L/C_D only increases marginally (around 4%) compared to the wing of an AR of 6. In addition, a wing with a higher aspect ratio will have a significantly higher deflection since the deflection is highly dependent on the span. To compensate for this, more structural weight must be used to support the wing, increasing the overall maximum takeoff weight of the aircraft. As a result, a higher aspect ratio of 7 or 8 is not suitable for the aircraft. Lower aspect ratios will reduce the bending moment at the attachment point of the wing, so less structural support is required, and a lower aspect ratio also improves the roll maneuverability of the aircraft. However, with an AR of 5, the wing will have increased induced drag, reducing the aerodynamic characteristics of the wing. Consequently, from the trade study, an aspect ratio of 6 was determined to be the best choice for the wing as it provides a good lift to drag ratio while retaining high structural characteristics.

To validate the aerodynamics of the wing design, the lift distribution of the wing with an AR of 6 was analyzed using XFLR5. As seen in Figure 4.3, the lift distribution is significantly close to the ideal elliptical lift distribution, with a mean square error of only 0.002. As a result, a rectangular wing with AR = 6 is sufficient for the aircraft.

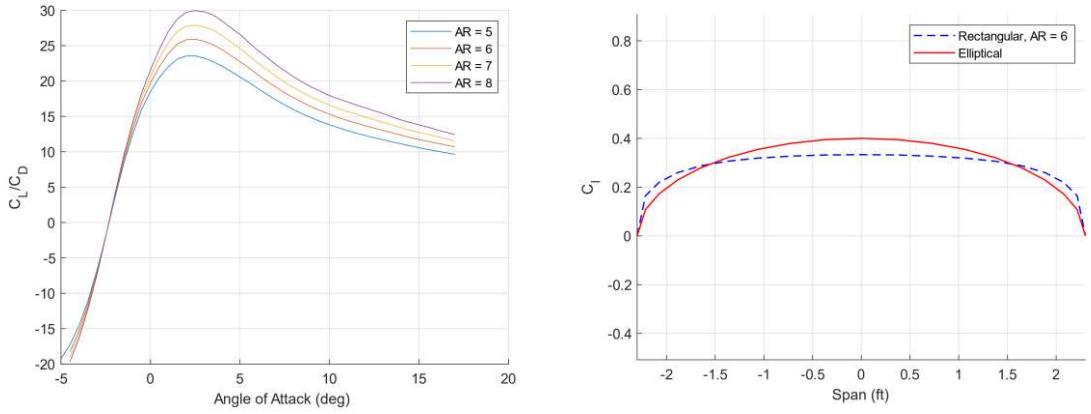

Figure 4.3: The C_L/C_D vs angle of attack of different AR (left) and the wing lift distribution (right)

With the aspect ratio decided and the required planform area known, the wingspan and the chord can be calculated as 4.66 ft and 0.777 ft, respectively. Using XFLR5, the lift curve for the wing was analyzed. The required cruise lift coefficient can be readily calculated from the estimated weight and targeted cruise velocity of 82 ft/s. Consequently, the setting angle for the wing was determined to be $1.5°$.

4.2.3 Tail Sizing

The horizontal tail was designed using the simplified non-dimensional longitudinal trim equation at cruise [1]:

$$C_{m_{o\_w}} + C_L(h - h_0) - \eta_H \bar{V}_H C_{L_H} = 0$$

where the tail volume coefficient is defined as:

$$\bar{V}_H = \frac{l}{c}\frac{S_H}{S}$$

With the initial sizing of the wing completed, the pitching moment coefficient was readily available using XFLR5 simulation results. The cruise lift coefficient was also determined prior. Additionally, the center of gravity of the aircraft was estimated using a schematic of the locations of the main components of the aircraft. Based on aircraft with similar configuration [1], a tail efficiency of $\eta_H = 0.9$ and a horizontal tail volume $\bar{V}_H = 0.5$ was assumed initially.

As a result, from the longitudinal stability equation, the lift coefficient C_{L_H} required for the tail was calculated as -0.0624. Additionally, the horizontal tail area was also calculated to be 0.937 ft^2 from the tail volume coefficient equation. An aspect ratio of 3 was chosen for the horizontal tail to increase structural strength since a thin airfoil (NACA 0009) was selected. The tail was simulated XFLR5 to obtain its lift curve, and the tail setting angle was calculated to be $-1°$ for cruise.

The vertical tail was designed similarly by assuming a vertical tail volume coefficient $\bar{V}_V = 0.04$. The vertical tail aspect ratio was chosen as 1.2, also due to structural considerations.

With the initial dimensions chosen, the wing, horizontal tail, and vertical tail were simulated in XFLR5 to study the static and dynamic stability of the aircraft. Multiple tail coefficients were also considered and simulated, as higher coefficients yielded a more stable aircraft with the cost of controllability. However, the initial values chosen were made to make the aircraft more controllable. With further test flights, the tail coefficients can be iterated based on pilot feedback to find the best values.

4.2.4 Control Surfaces Sizing

From the wing sizing, the aircraft can take off without flaps based on the XFLR5 simulation of the wing. However, the angle of attack required is $13°$, which is close to the stall angle. As a result, flaps were employed to increase the lift coefficient of the wing during takeoff and landing to avoid stalling. The span and chord of the flaps were initially simulated using a MATLAB script to predict the incremental lift

increases for the wing with certain flap configurations. After multiple iterations, initial values that ensure the lift coefficients required during takeoff and landing were obtained. The values were then used as a starting point for the wing model in XFLR5. From there, the final sizing for the wing flaps was achieved when the desired lift coefficient during takeoff and landing was reached. This resulted in the chord of the flap being 20% of the wing chord and the span of the flap being 60% of the wingspan. The flaps will be deflected $15°$ at takeoff, which only requires the aircraft to rotate nose up $10°$ during takeoff. This will ensure that the wing will not stall. For landing, the flaps will be deflected $25°$.

With the chord and the span of the flaps determined, the ailerons were chosen to occupy the remaining span of the wing. As a result, the chord of the ailerons was the same as the flaps (20% of the wing chord), and the span of the ailerons was 40% of the wingspan. Further simulations were conducted to confirm that the roll rate of the aircraft was acceptable during turns.

The elevator was designed in an equivalent manner to ensure the required takeoff rotation was achieved. The elevator chord was determined to be 25% of the horizontal tail chord, and the elevator span ran across the whole horizontal tail. The vertical tail was designed to ensure sufficient yaw control, which resulted in the chord of the rudder to 25% of the vertical tail, and the span of the rudder also occupies the whole span of the vertical tail.

4.2.5 Propulsion Sizing

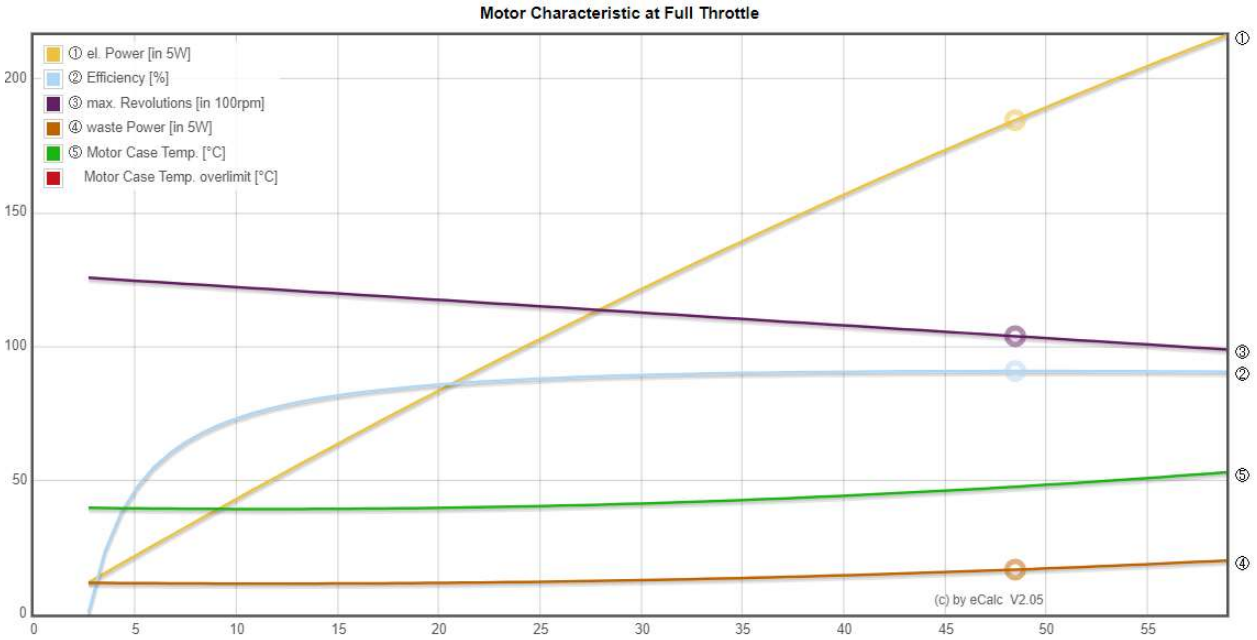

Figure 4.4: Characteristics of the motor at full throttle

Figure 4.5: Input data for motor characteristics

Battery		Motor @ Optimum Efficiency		Motor @ Maximum		Propeller		Total Drive		Airplane	
Load:	11.16 C	Current:	47.97 A	Current:	49.10 A	Static Thrust:	4238 g	Drive Weight:	1200 g	All-up Weight:	3629 g
Voltage:	19.25 V	Voltage:	19.04 V	Voltage:	18.97 V		149.5 oz		42.3 oz		128 oz
Rated Voltage:	22.20 V	Revolutions*:	10400 rpm	Revolutions*:	10346 rpm	Revolutions*:	10346 rpm	Power-Weight:	300 W/kg	Wing Load:	73 g/dm²
Energy:	97.68 Wh	electric Power:	913.5 W	electric Power:	931.3 W	Stall Thrust:	- g		136 W/lb		23.9 oz/ft²
Total Capacity:	4400 mAh	mech. Power:	830.5 W	mech. Power:	846.7 W		- oz	Thrust-Weight:	1.17 : 1	Cubic Wing Load:	10.3
Used Capacity:	3740 mAh	Efficiency:	90.9 %	Efficiency:	90.9 %	avail.Thrust @ 0 km/h:	4238 g	Current @ max:	49.10 A	est. Stall Speed:	39 km/h
min. Flight Time:	4.6 min			est. Temperature:	48 °C	avail.Thrust @ 0 mph:	149.5 oz	P(in) @ max:	1089.9 W		24 mph
Mixed Flight Time:	8.1 min				118 °F	Pitch Speed:	126 km/h	P(out) @ max:	846.7 W	est. Speed (level):	105 km/h
Weight:	600 g			Wattmeter readings			78 mph	Efficiency @ max:	77.7 %		65 mph
	21.2 oz			Current:	49.1 A	Tip Speed:	594 km/h	Torque:	0.78 Nm	est. Speed (vertical):	21 km/h
				Voltage:	19.25 V		369 mph		0.58 lbf.ft		13 mph
				Power:	945.2 W	specific Thrust:	3.97 g/W			est. rate of climb:	10.6 m/s
							0.14 oz/W				2093 ft/min

share performanceCalc add to >> Download .csv (0) << clear

Motor Partial Load

Propeller	Throttle	Current (DC)	Voltage (DC)	el. Power	Efficiency	Thrust		Spec. Thrust		Pitch Speed		Speed (level)		Motor Run Time
rpm	%	A	V	W	%	g	oz	g/W	oz/W	km/h	mph	km/h	mph	(85%) min
1400	11	0.3	22.2	5.8	36.0	78	2.7	13.3	0.47	17	11	-	-	850.6
2100	17	0.6	22.2	12.8	55.3	175	6.2	13.6	0.48	26	16	-	-	386.9
2800	23	1.1	22.1	24.7	68.1	310	10.9	12.6	0.44	34	21	-	-	200.4
3500	28	2.0	22.1	43.1	76.1	485	17.1	11.3	0.40	43	27	-	-	114.4
4200	34	3.2	22.0	69.7	81.2	698	24.6	10.0	0.35	51	32	-	-	70.4
4900	40	4.9	21.9	106.4	84.5	951	33.5	8.9	0.32	60	37	-	-	45.9
5600	47	7.2	21.8	154.8	86.7	1241	43.8	8.0	0.28	68	42	54	34	31.3
6300	53	10.1	21.6	216.6	88.2	1571	55.4	7.3	0.26	77	48	64	40	22.2
7000	60	13.9	21.4	293.7	89.3	1940	68.4	6.6	0.23	85	53	71	44	16.2
7700	67	18.6	21.1	387.8	90.0	2347	82.8	6.1	0.21	94	58	78	48	12.1
8400	75	24.4	20.7	500.8	90.5	2793	98.5	5.6	0.20	102	64	85	53	9.2
9100	**83**	**31.7**	**20.3**	**634.5**	**90.8**	**3278**	**115.6**	**5.2**	**0.18**	**111**	**69**	**92**	**57**	**7.1**
9800	92	40.6	19.8	790.7	91.0	3802	134.1	4.8	0.17	120	74	99	62	5.5
10346	100	49.1	19.3	931.3	90.9	4238	149.5	4.6	0.16	126	78	105	65	4.6

Figure 4.6: Input data for motor characteristics (Continued)

Using initial projections for weight, wingspan, wing area and drag including the desired battery properties, an open-source software called eCalc was used to sort through common manufacturers that were used to form a list of possible motor and propeller combinations. The E-Flight Power 52 Brushless Outrunner Motor was chosen alongside the 12” x 8” propeller as this motor and propeller combination provided the desired thrust/weight ratio. The theoretical performance of this motor is shown by Figure 4.4 which depicts the eCalc graph followed by Figure 4.5 and 4.6 which shows the inputs used to calculate this.

The battery chosen for the aircraft is a 6S 22.2V 4400mAh LiPo battery, however the space in which we work restricts the batteries we work with to less than 18V, a 4S 14.8V 4000mAh LiPo battery was chosen

to perform tests, this battery will also provide desired performance results in the event of that the gross take-off weight reduces from 7.24lb to 6lb. LiPo batteries were chosen over NiMH batteries for both instances because of the higher energy density and power that LiPo's provide.

4.2.6 Uncertainties

Most of the lift estimation of the wing and tail were analyzed using the inviscid model in XFLR5. Even though the velocity of the aircraft is well below Mach 0.3 (the incompressible fluid assumption limit), there will be discrepancies between the calculated and the actual value. In a similar manner, the drag analysis was also conducted using an empirical method; though it provided acceptable results, if a full CFD simulation was conducted on the aircraft, more accurate data for both the lift and drag coefficients can be acquired. In addition, the stability analysis did not include the simulation of the fuselage; therefore, there could be errors in the estimations of the static and dynamic stability.

4.3 Design Trade Studies

4.3.1 Drag Analysis

The drag for the aircraft was estimated using Hoerner's [2] component drag contribution method:

$$C_{D_P} = \frac{KC_f S_{wet}}{S_{ref}}$$

The wing and empennage drag was initially calculated using the method; however, these components' drag was later replaced with more accurate values from the XFLR5 simulation.

For the fuselage, the form factor is a function of the fineness ratio (the ratio of the length over the diameter). Though the fuselage had a trapezoidal cross-section, an equivalent diameter was used to model the fuselage as a cylinder to calculate the corresponding drag contribution.

The wheels for the landing gear were modeled as a cylinder perpendicular to the airflow to estimate the drag coefficient, and the remaining part was modeled as a flat plate.

The breakdown for the drag contribution is shown in Table 4.2 and Figure 4.7. Since the payloads are situated within the fuselage, the drag contribution for all three missions was similar.

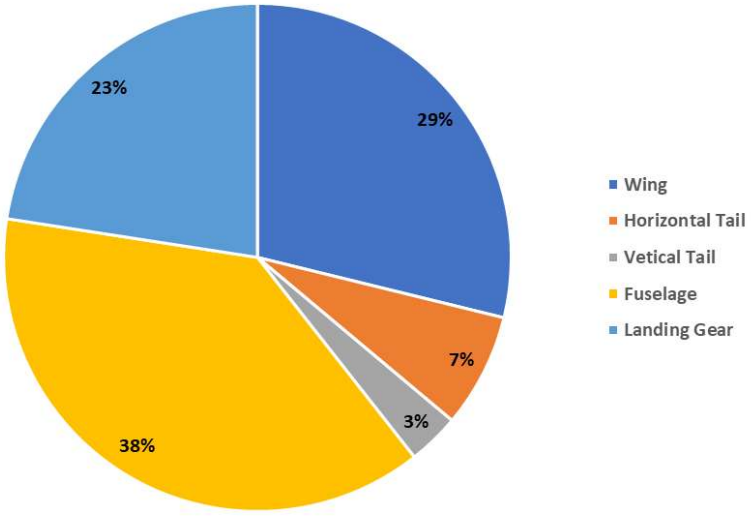

Figure 4.7: Pie chart for parasite drag coefficient

Table 4.2: Parasite drag coefficient of the components

Component	C_{D_P}
Wing	0.00856
Horizontal Tail	0.00216
Vertical Tail	0.000980
Fuselage	0.0113
Landing Gear	0.00670
Total	0.0297

4.4 Stability Analysis

4.4.1 Static Stability

To confirm the design for the horizontal tail and the vertical tail, static stability analysis was conducted in XFLR5, with the relevant non-dimensional stability derivatives shown in Table 4.3. The location of the CG was estimated using the CAD model with components mounted on the fuselage, and it was iterated to achieve stable values for the derivatives.

Table 4.3: Non-dimensional stability derivatives for the aircraft

C_{L_α}	5.08	C_{L_u}	-0.005	C_{L_q}	10.2	C_{l_β}	-0.028	C_{l_p}	-0.464	C_{l_r}	0.112
C_{m_α}	-1.50	C_{m_u}	-0.002	C_{m_q}	-10.9	C_{n_β}	0.148	C_{n_p}	-0.005	C_{n_r}	-0.112
C_{X_α}	0.153	C_{X_u}	-0.034	C_{X_q}	0.146	C_{Y_β}	-0.441	C_{Y_p}	0.001	C_{Y_r}	0.339

As seen in Table 4.3, the two most important derivatives for the horizontal tail C_{m_α} and C_{m_q} are both negative, indicating that the aircraft is longitudinally stable. Furthermore, the C_{n_β} is positive and the C_{n_r} is

negative, which shows that the aircraft is laterally stable. As a result, from the XFLR5, the aircraft has achieved static stability, with a static margin of 29%. However, the stability and controllability of the aircraft will also be further iterated and confirmed with later test flight and pilot feedback.

4.4.2 Dynamic Stability

The dynamic stability [5] of the aircraft during cruise conditions was studied simultaneously using the XFLR5 simulation Figure 4.8. The root locus was used to analyze the two longitudinal dynamic stability modes (short period and phugoid) and the three lateral dynamic stability modes (roll, Dutch roll, and spiral). Since the syringes for mission 2 have negligible weight compared to the whole aircraft, the CG would not be shifted significantly. Furthermore, for mission 3, the vaccine package will be stationed close to the CG of the empty aircraft; hence, the CG for mission 3 will also be like the first two missions. Accordingly, the dynamic stability analysis for all three missions had similar results shown in the root locus plot in Figure 4.8.

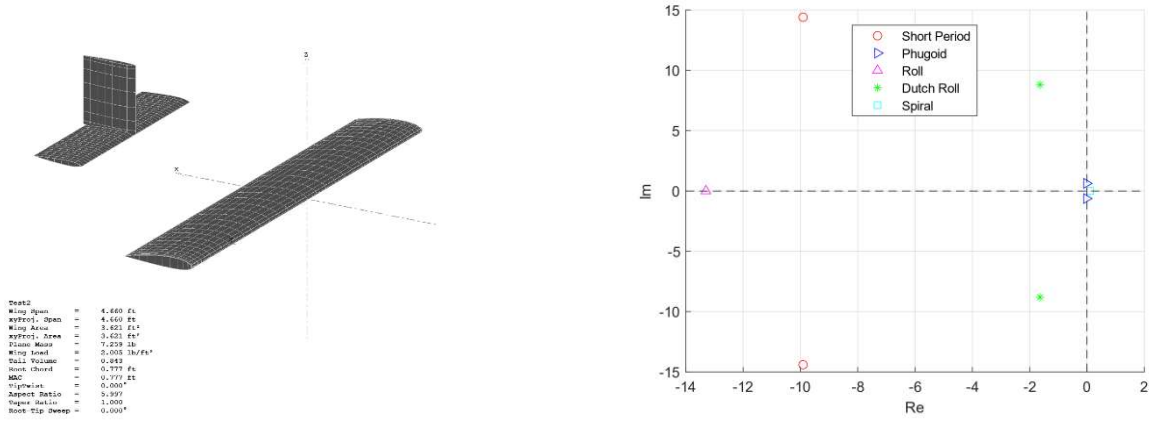

Figure 4.8: XFLR5 simulation of the aircraft (left) and root locus plot of the stability modes (right)

As seen in Figure 4.8, except for the spiral, all the other modes have a negative real component; thus, these modes are dynamically stable for these modes. On the other hand, the spiral mode is unstable. However, the time to double the amplitude of the mode was 6.25 seconds; this was determined to be sufficient for the pilot to apply correction to manually stabilize the aircraft. As a result, the XFLR5 simulation showed that the dimensions for the aircraft satisfy the dynamic stability requirements. Table 4.3 shows all the characteristics of dynamic stability modes. Additionally, further simulations for dynamic stability were also considered based on the pilot feedback from the test flights.

Table 4.3: Parameters for the dynamic stability modes

Modes	Longitudinal		Lateral		
	Short Period	Phugoid	Roll	Dutch Roll	Spiral
$\omega_n (rad/s)$	17.6	0.628	-----	8.96	-----

$\omega_d (rad/s)$	14.4	0.628	-----	8.80	-----
ζ	0.568	0.028	-----	0.183	-----
$\tau\ (s)$	0.101	57.8	0.075	0.610	9.03

4.5 Mission Performance

With the preliminary sizing for the aircraft components, the three mission performances can be estimated from the calculated aerodynamics characteristics. With the targeted cruise speed of 82 ft/s and the total flight range calculated as 3610 ft, the ideal time to complete mission 1 was 44 seconds. However, more time was added to account for difficulties that may occur during takeoff and landing. Additionally, it is also hard for the pilot to keep a constant speed and follow the flight path perfectly; as a result, the total time estimated for mission 1 was estimated to be 70 seconds. For mission 2, with the introduction of the syringes, the stability of the aircraft might change slightly; as a result, the time estimated to complete the flight path was around 80 seconds. Finally, since the weight of the aircraft for mission 3 is like mission 2, the flight characteristics did not change drastically. Furthermore, since the design of the aircraft was focused on the maximum takeoff weight for mission 3, the aircraft is predicted to complete the vaccine deployment. All the flight characteristics and predicted mission scores are shown in Table 4.4.

Table 4.4: Predicted flight characteristics and mission performance

	Mission 1	Mission 2	Mission 3
$C_{L_{max}}$	1.21	1.29	1.30
$C_{L_{cruise}}$	0.244	0.260	0.262
C_{D_P}	0.0297	0.0297	0.0297
$(L/D)_{cruise}$	8.22	8.75	8.82
$Total\ Weight\ (lb)$	6.74	7.18	7.24
$W/S\ (lb/ft^2)$	1.86	1.98	2.00
$V_{stall}\ (ft/s)$	35	35	35
$V_{cruise}\ (ft/s)$	82	82	82
$Lap\ Time\ (s)$	70	80	-----
$Syringes$	-----	10	-----
$Vaccine\ Package$	-----	-----	1
$Mission\ Score$	1	1.13	2.33

5.0 Detail Design

Detail design was the final step before fabrication of the entire system and further detailed design of specialized subsystems such as the deployment mechanism and integrations. Fabrication includes the

full structural assembly of the wing, fuselage, motor mount system, landing gear, tail, and specialized subsystem components. Iterative design for performance improvement continued through the manufacturing process to adapt to material availability and design challenges.

5.1 Dimensional parameters

Table 5.1 lists characteristics parameters for the aircraft.

Table 5.1 - Dimensional parameters

Overall Dimensions		**Elevator**		**Tail**	
Length	56.1 in.	Span	21 in.	Airfoil	NACA 0009
Width	56 in.	Max angle	30°	Horizontal span	21 in.
Height	26.5 in.	Chord	7 in.	Vertical Span	14 in.
Motor		**Fuselage**		Vertical Area	0.45 ft^2
Model	E-Flite Power 52	Total Length	48 in.	Horizontal Area	0.94 ft^2
Effective Kv	590 rpm/V	Nose Length	52.4 in.	Tail Arm	32 in .
Power Rating	931 W	Width	8 in.	**Wing**	
Propeller	12 in. x 8 in.	Height	6 in.	Airfoil	NACA 2415
Landing Gear		**Rudder**		span	56 in.
Overall Height	6 in.	Span	14 in.	AR	5
Wheelbase	13 in.	Max angle	30°	Platform Area	3.62 ft^2
Wheel Diameter	2 in.	Chord	7.5 in.	Incidence Angle	1.5°
				Chord	9.5 in.

5.2 Structural characteristics

Primary loading considerations for the structure design were weight, aerodynamic, and propulsive loads. To ensure the structural stability of the aircraft, the super structure was designed such that all loads had a path to the main loadbearing structural components of the aircraft as depicted in Figure 5.1

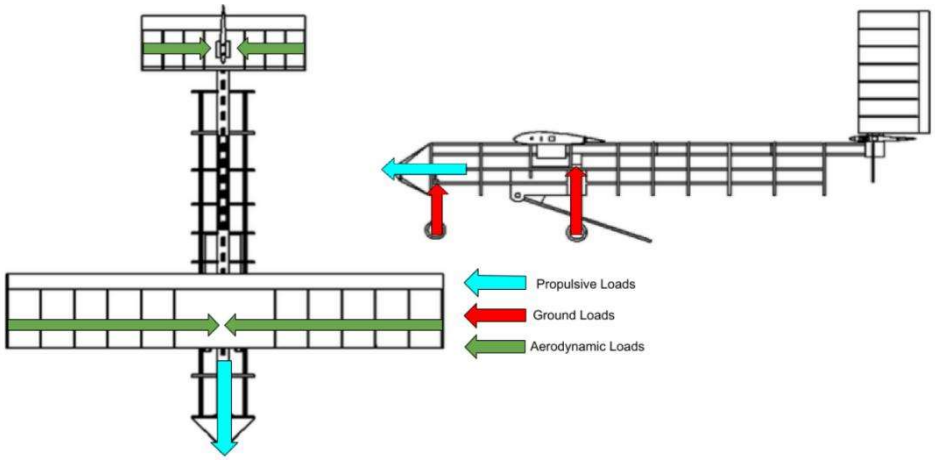

Figure 5.1: Loadbearing Analysis

The primary loadbearing structural component of the aircraft is a spar that spans the length of the aircraft. The spar was modeled after an I-beam which would resist bending due to loads on the aircraft.

5.2.1 Wing design

The wing has a span of 56 inches and a chord of 9.5 inches including a default angle of attack of 1.5 degree, giving its airfoil the NACA 2415 optimal conditions for the size of the aircraft. This is accomplished with a 3D-printed PLA bracket and a ½ inch wooden spar which is comprised of two 36-inch-long square dowels bonded together with adhesive. Due to limitations experienced by the manufacturing team during initial prototyping, it carried through to the final iteration of the wing. The spar is located at the center of gravity of the ribs to provide enough structure and the most efficient way to transfer load to the spar from the ribs of the wing.

Figure 5.2 NACA2415 Wing

5.2.2 Tail Design

The design for the tail utilized a NACA 0009 airfoil. This airfoil was selected because of its symmetrical shape and low drag to lift ratio. The symmetrical geometry allows for more predictable behavior when control surfaces are used to adjust flight paths. The tail was manufactured the same way as the wing and with the same considerations concerning material availability. The tail uses a similar bracket to that of the wing but also holds the rudder in place. The rudder is similar in composition to the tail using the NACA0009 airfoil to control the movement of the aircraft during flight to influence flight path. Both the rudder and elevators are designed to allow for 30 degrees of motion to help control the aircraft during flight. This motion is controlled through small plastic gear servos mounted inside of each side of the tail and inside of the rudder.

Figure 5.3: Aircraft Tail Section

5.2.3 Fuselage Design

The fuselage is comprised of a main structural I-beam and several ribs to give the desired shape of the aircraft. This shape is to accommodate the payload required in the second and third missions. The I-beam is not only structural for the fuselage but handles all the loads from other subsystems such as the wing, deployment mechanism, and landing gear. It was determined that the internal cavity of the fuselage must be at least 4 inches by 4 inches to accommodate the payloads and payload delivery system. As such, the fuselage ribs were designed to accommodate this space. The ribs, additionally, were designed to provide enough material to survive the load applied to them via the deployment mechanism and the payloads during flight, including the forces applied by the propulsion system.

5.2.4 Propulsion Design

The main components of the propulsion system consist of a motor, ESC, fuse, two batteries, and a flight controller. As stated in the preliminary design section, the E-Flite Power 52 Brushless Outrunner Motor uses the 12” x 8” propeller. The Spektrum AR620 flight controller was used due to its proven results over the past few years. The 80 Amp Spektrum ESC was selected as the ESC due to its relatively lightweight build, onboard heatsink which keeps the system cooler and to mitigate compatibility issues between the ESC and the chosen receiver. A 60Amp inline blade fuse is used to satisfy the requirement put forth by the rule book.

5.2.5 Syringe Packing

A cloth bag with a circular bottom with a diameter of 4.5 inches and a height of 5 inches will be used for packaging the syringes. The cloth will act as the loop side of Velcro and will mate with the hook side on the interior wall of the fuselage. Seen in Figure 5.4, a net bag was considered but the holes slowed down syringe loading.

Figure 5.4: Initial Cloth Bag

5.3 Drawing Package

The following drawing package includes a dimensional structural arrangement of the aircraft in its configuration for Missions 1, 2, and 3.

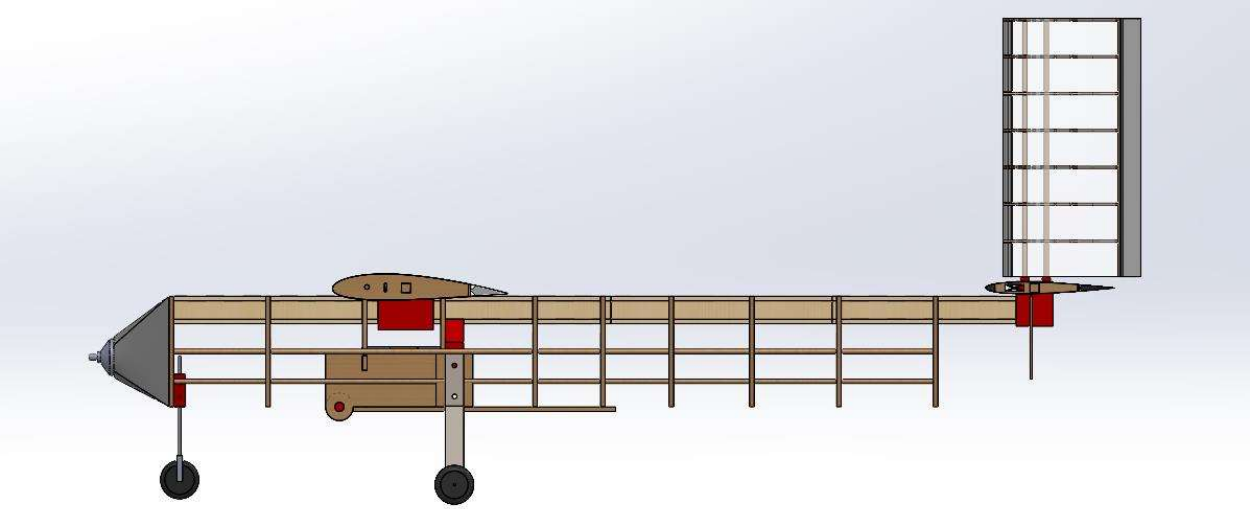

Figure 5.3.1: RH-01 Mission 1 No Payload

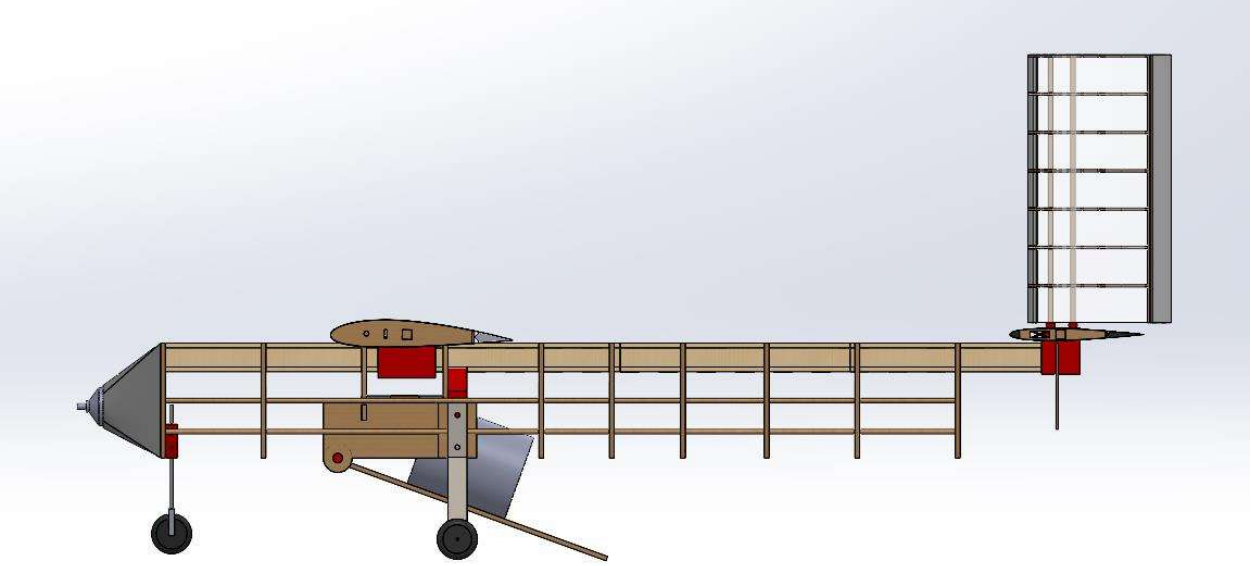

Figure 5.3.2: RH-1: Mission Two Syringe Delivery

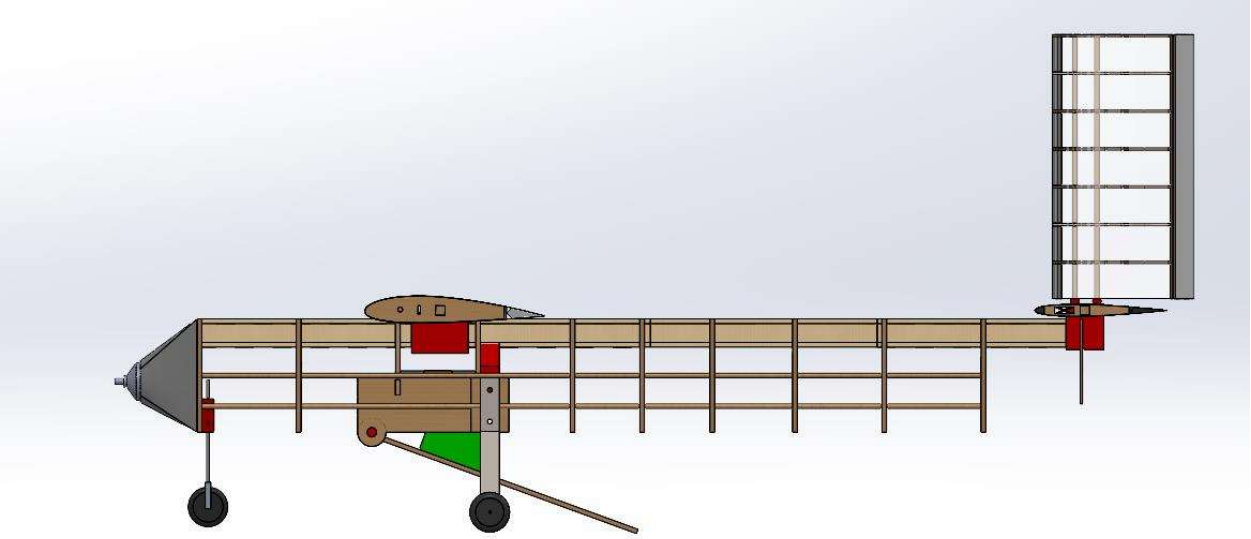

Figure 5.3.3: RH-1: Mission 3 Vaccine Vial Delivery

6.0 Manufacturing Plan

The materials used to construct aircraft are the following: MonoKote, Balsa Wood, Pure bond Plywood, Foam and Aluminum. These materials molded alongside the available manufacturing processes were examined to build the wings, fuselage, tail and deployment mechanism. The team prioritized off-the-shelf components to reduce areas of failure, decrease manufacturing time whenever possible, and efficiently spend the available funding of materials.

6.1.0 Manufacturing Process

The following sections highlight the available manufacturing methods for the UML AIAA-DBF team.

6.1.1 Laser-Cutting

Laser cutting is a resource the team is familiar with and comfortable using. This technique allows rapid prototypes of various mechanisms and offers higher dimensional precision compared to the other manufacturing techniques. Laser cutting was used extensively due to most of the aircraft being comprised of balsa wood and pure bond plywood due to their ability to support critical structural loads in the fuselage, wing, tail, and deployment mechanism.

6.1.2 Hot Wire Foam Cutting

EPP (expanded polypropylene) and EPS (extruded polystyrene) foams are flexible, light, and easy to cut for rapid prototyping. To cut foam, a 5-axis CNC hot wire foam cutter was used to test various airfoils and leading edges to validate design choices for the structure of the aircraft.

6.1.3 3D-Printing

Additive manufacturing is one of the most versatile methods of manufacturing complex parts in a short amount of time, which allows for rapid prototyping of different mechanisms. Most of the 3D-printed parts that were used in the construction of the aircraft did not require high resolution. Therefore, a Prusa MK3 Fused Deposition Molding (FDM) printer was used. The team also had access to a Formlabs Stereolithographic (SLA) printer when high resolution and smooth surface finishes are required. This method was used to 3D-print a bracket to connect the wing to the fuselage on the prototype aircraft. In addition, this method of manufacturing was used to create a bracket, engine mount, and shroud of the aircraft.

6.1.4 MonoKote Covering

MonoKote is a film product to seal the structure of the aircraft's surface to create the correct geometry with the addition of little weight. This product was used extensively in our aircraft for sealing the wing, control surfaces, tail and fuselage. This allowed the wing control surfaces and tail to generate lift and control the airflow during flight when the aircraft is in motion. The fuselage coating improves the aerodynamics while leaving an aesthetic finish.

6.1.5 Adhesives

The adhesives used to assemble the aircraft were wood glue and 5-minute epoxy. Wood glue was used to bond the laser cut wood parts due to their cost effectiveness and ease of use. Epoxy was used in minimal capacity due to EHS regulations in our workspace pertaining to the fumes produced. Due to this limitation, epoxy was only used to fuse the two pieces of the spar together.

6.2.0 Manufacturing Process for Major Aircraft Components

Given the information above, the following subsections outline the manufacturing methods used in the construction of each major aircraft component:

6.2.1 Wing

The wing is comprised of ribs, a main spar, a support spar, a mounting plate and is coated with a thin heat-shrink plastic layer called MonoKote. The spar is built using two off-the-shelf square ½ inch wooden dowels each 36 inches long. This made design and manufacturing simpler because they could be purchased and required few alterations to achieve the desired length. To achieve the 56-inch wingspan, the dowels were cut and joined using epoxy. The cut was placed at the middle of the wing inside of the bracket to give it the maximum amount of support to handle the load applied during flight, especially during maneuvers and climbing flights where the aerodynamic loads are at their highest. To secure the wing to the main I-beam, a bracket was designed to hold the wing in place. The bracket is removable so that the wing is not permanently attached to the I-beam and in the event of a crash during testing, it can be replaced easily. This bracket is made of PLA and is bolted together using nylon nuts and bolts. Nylon

was chosen because of its lightweight and because of its resistance to shear force. The ribs of the wing were made using the NACA 2415 airfoil cut out of 1/8th inch plywood and balsa wood sheets using a laser cutter. Three cuts were made to the interior of the ribs; one for the main spar, one to accommodate a connector for the servo motors that will be housed inside of the wing, and one for a secondary support spar. The secondary support spar was added to increase the rigidity of the wing because of its relatively long wingspan. The support spar is made of a ¼ inch round wooden dowel.

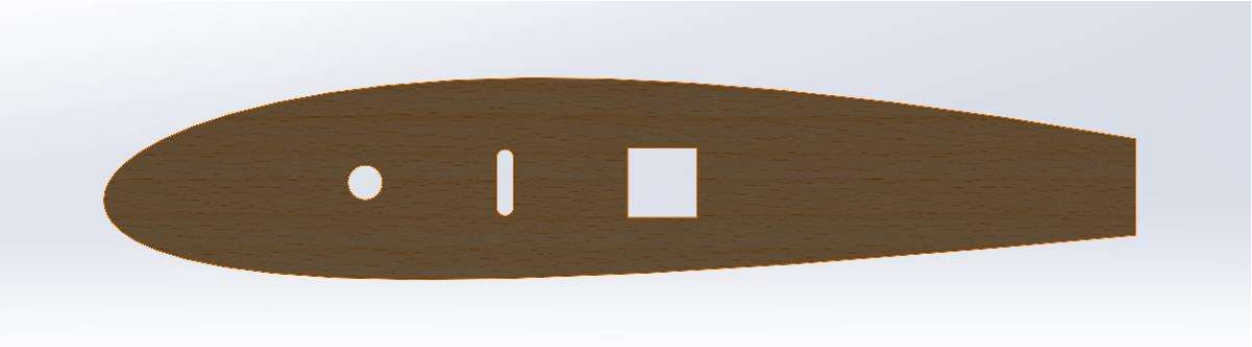

Figure 6.1: NACA2415 Rib Profile

6.2.2 Tail

The tail is comprised of two subsystems, the elevators and the rudder. Both are attached to the main I-beam using a 3D printed bracket and are also held together by nylon hardware. The elevators are made using the same square ½ inch wooden dowels as the wing and are made using the NACA 0009 airfoil. This shape makes up the ribs of the elevator with a 7-inch chord. The same geometry was also exported to a 5-axis CNC hot wire foam cutter to create the leading edge and the control surface. This was chosen because the foam provided the required rigidity while decreasing the weight of the subsystems as well as making repeatability for prototyping fast and reliable. To attach the control surfaces to the tail, the same method was followed as such for the wings, small segments of a ridged cloth were inserted into cuts made in the mounting plate and control surface then super glue was applied to lock the components in place. This provided a lightweight and effective hinge for the elevators and rudder.

6.2.3 Fuselage

The fuselage is based on a 48-inch-long I-beam spar that serves as the main component to the aircraft's body. To add structure, fuselage plates for the front, middle, and rear of the body are designed with square ½ inch wooden dowels insertion and an I-beam attachment. These fuselage plates act as structures to also provide spacing in the aircraft's body for later subassemblies. Then, the plates and fuselage spar were manufactured via laser cutting using 1/8th inch pure bonded plywood. With ease of integration in mind, the fuselage design considers the assembly process other subgroups have for the aircraft.

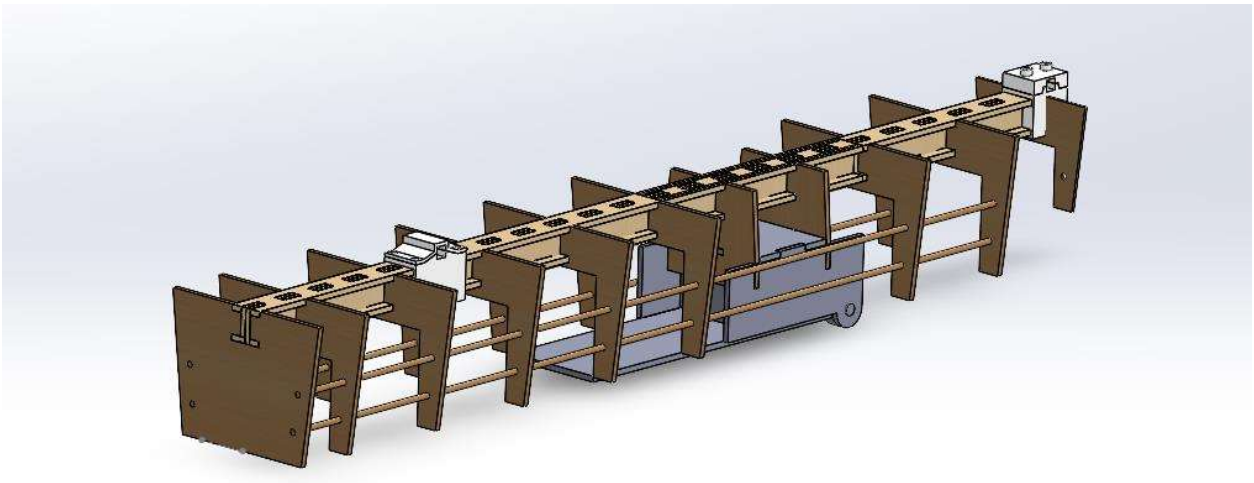

Figure 6.2: Aircraft Fuselage Assembly Layout.

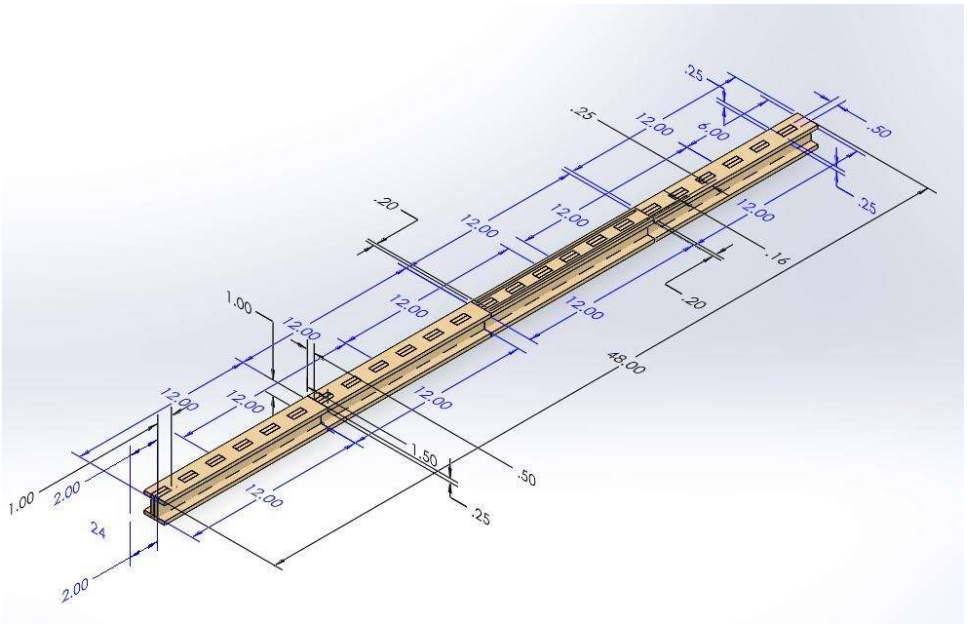

Figure 6.3. I-Beam Fuselage Spar.

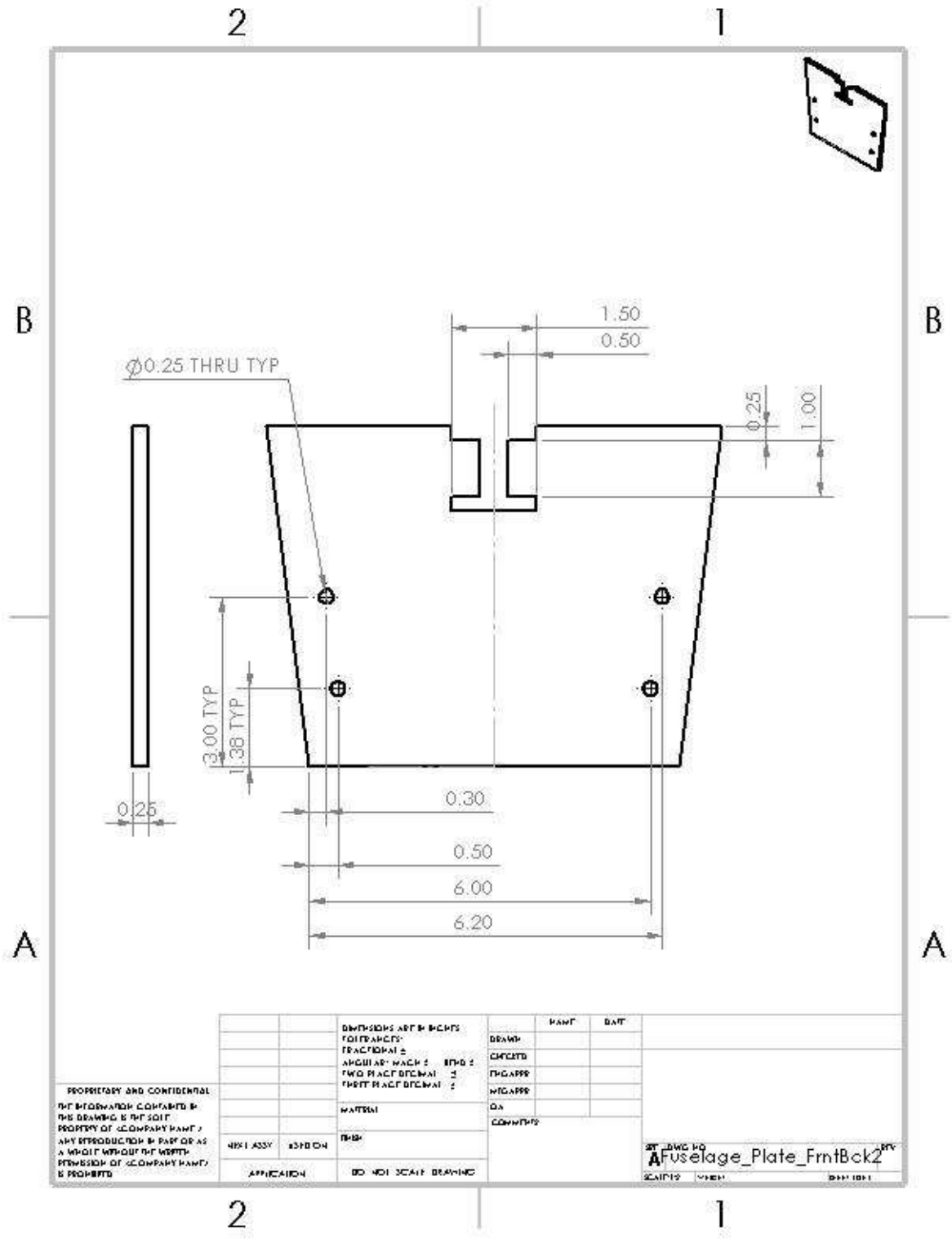

Figure 6.4: Front Fuselage Plate.

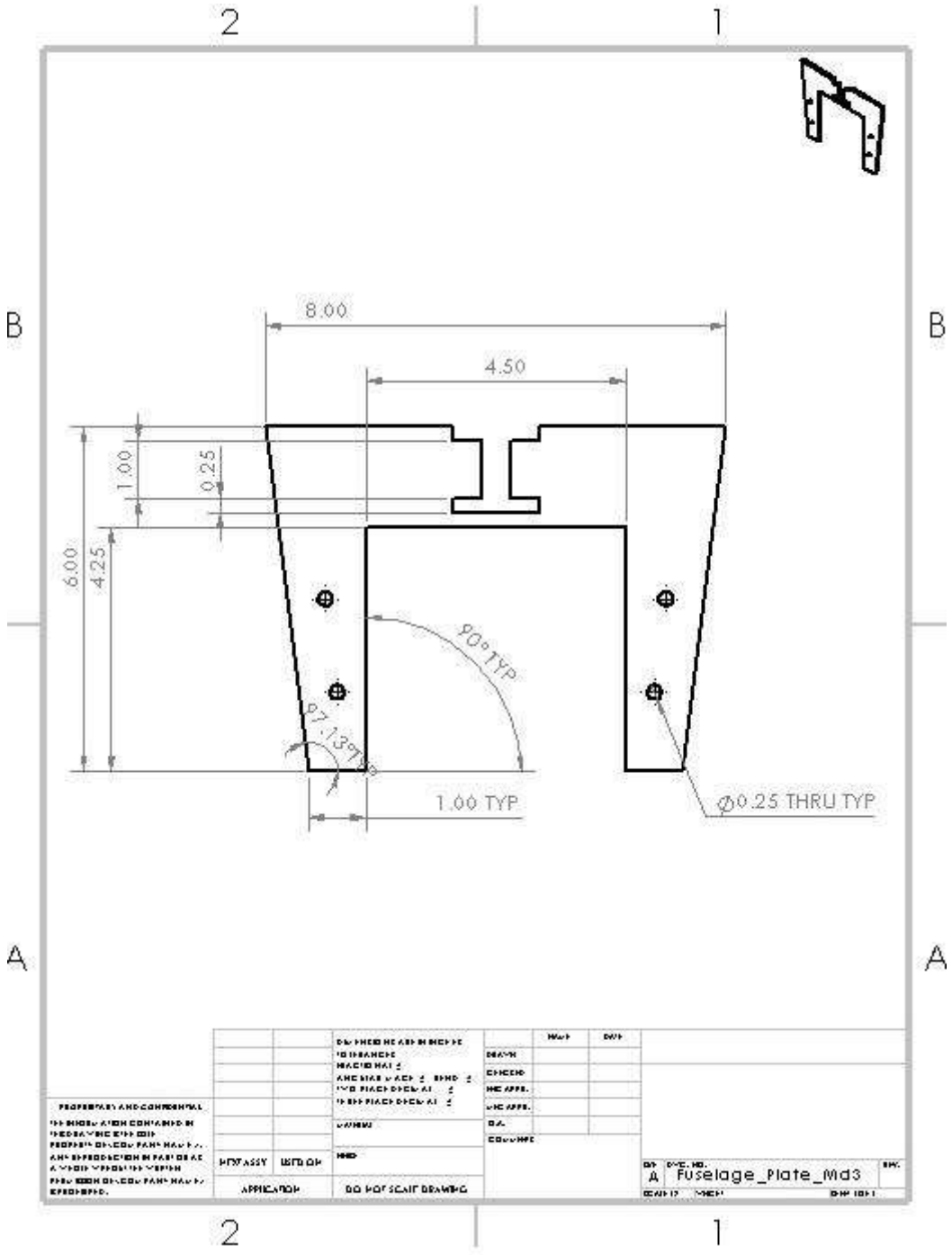

Figure 6.5: Middle Fuselage Plate.

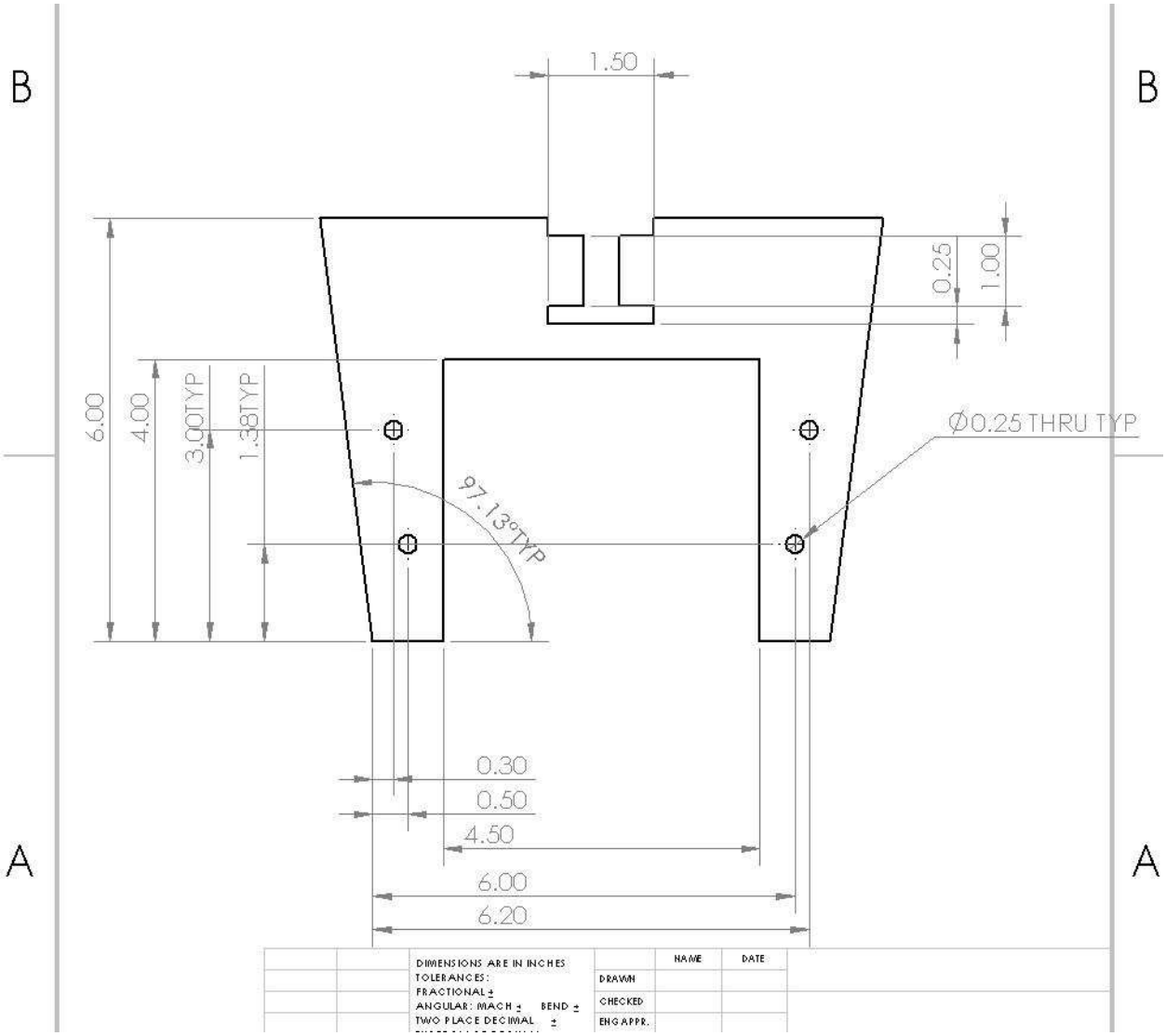

Figure 6.6: Second Middle Fuselage Plate.

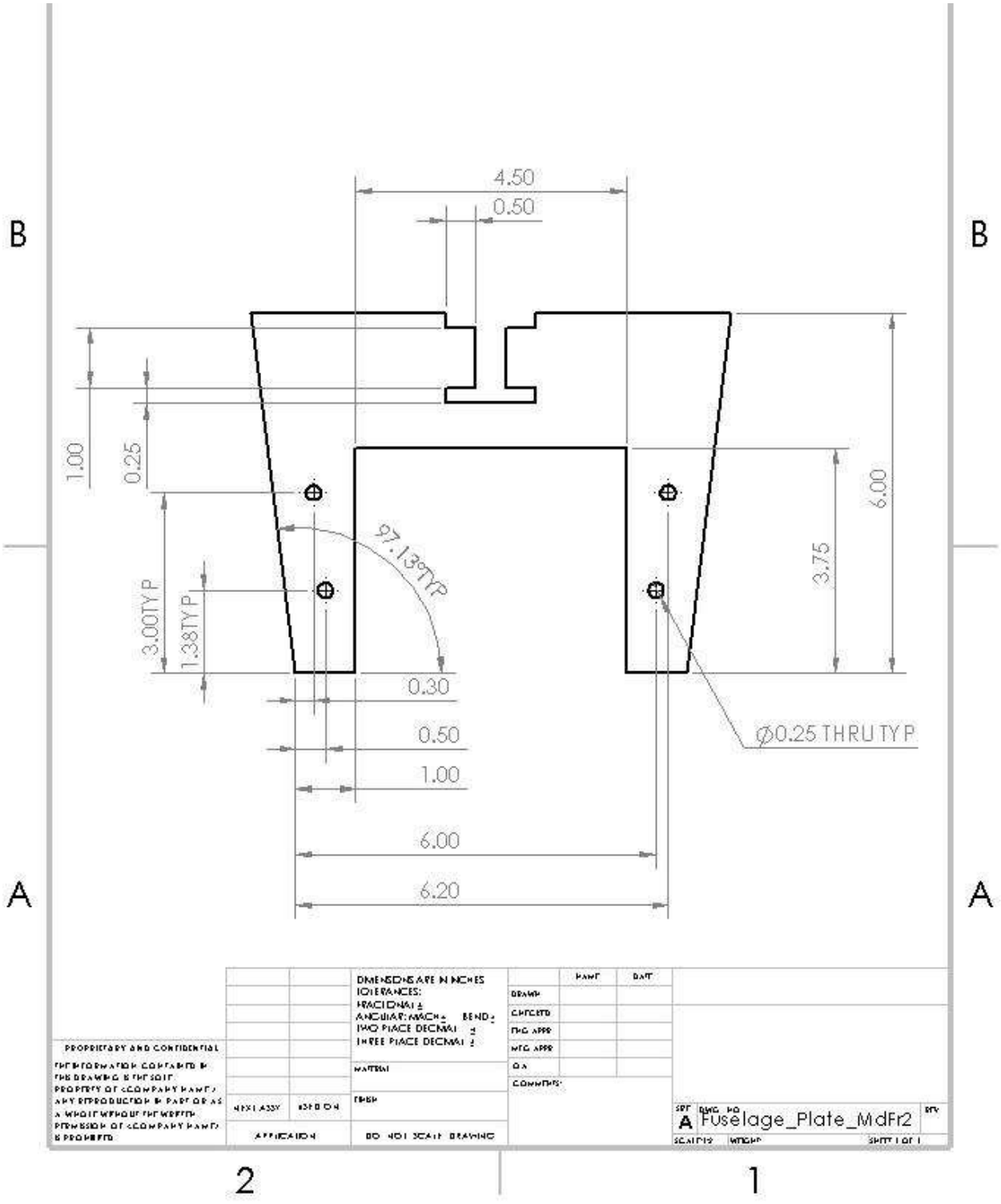

Figure 6.7. Rear Fuselage Plate.

6.3.0 Manufacturing Timeline

A Gantt chart, depicted in Table 6.1, was created the schedule of the manufacturing of each subsystem.

Table 6.1. manufacturing Timeline Gantt chart

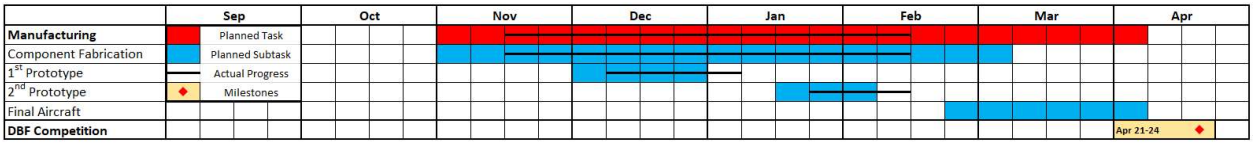

7.0 Testing Plan

The UML AIAA DBF team plans to do comprehensive ground and flight tests throughout the design and assembly processes. The team plans to test every minute mechanical system as they are built. After ensuring that each part works as designed, the team will assemble the aircraft. After the assembly, the aircraft will go through a rigorous flight test including flight time, maximum payload carried by the aircraft, lift for takeoff, pilot inputs, deployment system, glide time without power, and power consumption. All the tests will be done in an iterative manner. After the crucial inputs from the tests, minute critical changes will be made to the aircraft. The schedule for testing is outlined in Table 7.

Table 7.1 Gantt chart for testing

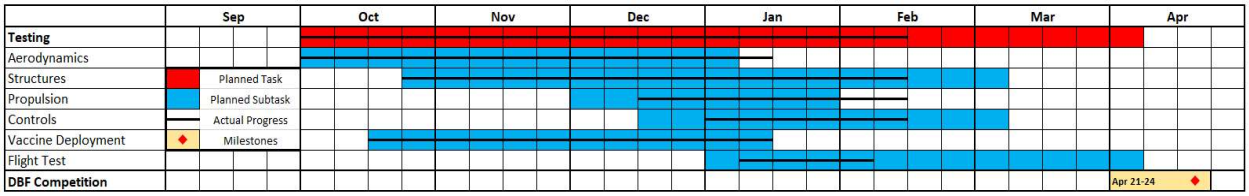

7.1 Test Objectives

Individual testing was performed on individual subsystems to validate their expected performance and meet design requirements.

- **Static Thrust Test**
  - Collect throttle, power, air speed data during ground and flight tests to validate the propulsion system
- **Point Load Test**
  - Conduct wing and fuselage loading tests to verify that the wind holds maximum lateral force
  - Obtain the value of the maximum load the main fuselage spar can withstand
- **Wingtip Test**
  - Validate wing's ability to support the aircraft's weight
- **Vial Package Deployment**
  - Verify the deployment mechanism can release the vaccine vial package without tripping its sensors

- Subject the deployment mechanism to simulated flight loads to ensure payload sensors aren't tripped

- **Payload Integration Testing**
  - Record time taken to load Syringes and Vaccine Vial Package
  - Optimize loading method

7.2.0 Subsystem Testing

7.2.1 Static Thrust Test

Once the propulsion requirements had been set by the design team, a trial propulsion system was assembled using validated batteries, motors, and ESCs. The first iteration of the system broke the 3D-printed joint due to excessive force from the motor. So, for the next few iterations, a new 3D printed joint was made which was 60% stronger than the first iteration. For the tests, battery voltage, current, battery time was closely monitored.

Figure 7.1: Thrust Test Apparatus

7.2.2 Point Load Testing

A sample section of the wing was manufactured and subjected to a point load to validate its ability to withstand expected flight loads. The point load was applied at the wing spars center by a manual point load machine as depicted in Figure 7.2. During testing, the max load the sample withstood was gathered by a loadcell placed above the point at which the load was being applied. Additional aspects of the sample such as failure points and propagation of cracks prior to total failure were monitored.

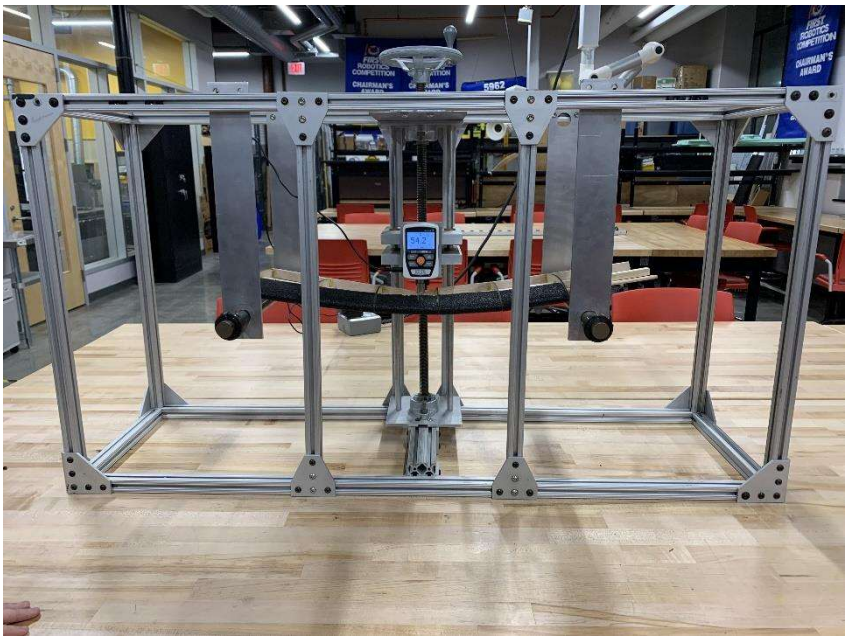

Figure 7.2: Wing-Spar Loaded in Point Load Tester

A sample section of the main fuselage spar was manufactured and placed into the point load tester. The point load was applied at the samples center by a manual point load machine as depicted in Figure 7.3. During testing, the max load the sample withstood was gathered by a loadcell placed above the point at which the load was being applied. Additional aspects of the sample such as failure points and propagation of cracks prior to total failure were monitored.

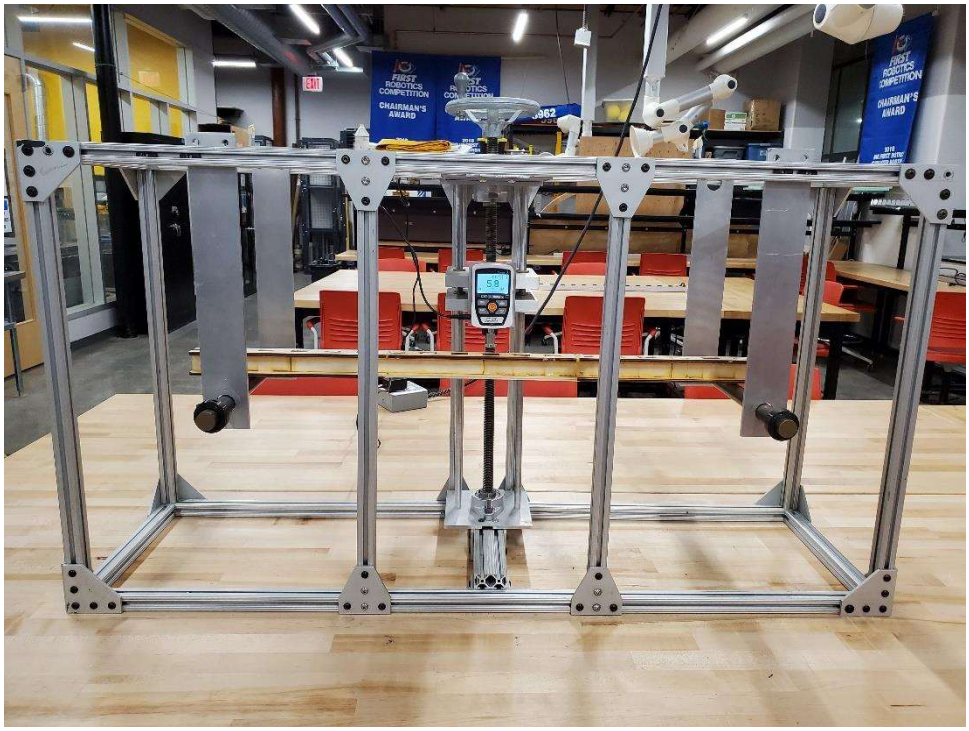

Figure 7.3: Fuselage I-Beam Spar Loaded in Point Load Tester

7.2.3 Wing Tip Test

To ensure the wing would pass preflight inspections, a wing tip test will be conducted prior to any flights of the prototype or final aircraft by supporting the entire crafts weight on the tips of the wings. This test will be performed on the aircraft when it is in its heaviest configuration.

7.2.4 Vial Package Deployment

To better characterize the loads required to trip the payloads sensors a version of the payload was manufactured as depicted in Figure 7.2.4. The package was designed to the upper limits of the weight and sizing tolerances to ensure all testing was performed was within its maximum possible tolerances. A 25G sensor was placed along each axis of the package to best simulate the veil package to be provided during the competition.

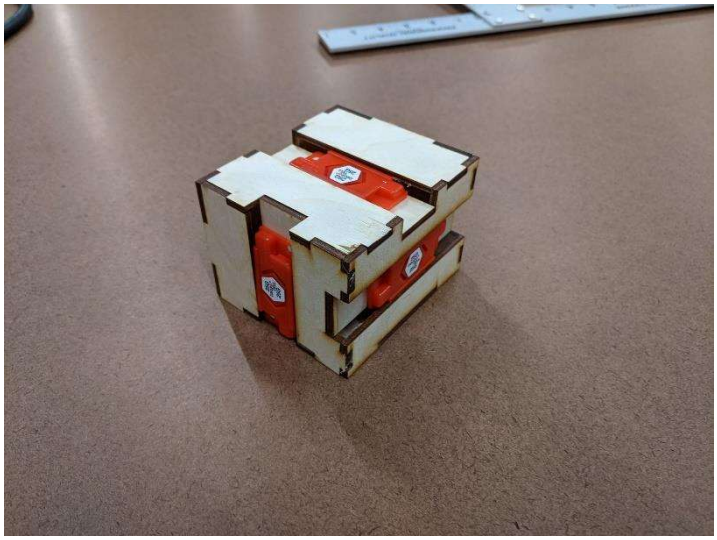

Figure 7.4: Vaccine Vial Package simulator

The Vaccine Vial Package was then subjected to several simulated loadings to characterize forces required to trip the sensors. Initial testing performed was simple drop tests to measure the maximum height the payload could fall without tripping sensors. Simulated deployments were then performed by sliding the vial package down a ramp as depicted in Figure 7.5. The inclination and length of the ramp were altered between testing to find the optimal configuration of the ramp. The ramp used for testing was made of the same material used to manufacture the flight deployment mechanism to ensure similar surface friction during deployment.

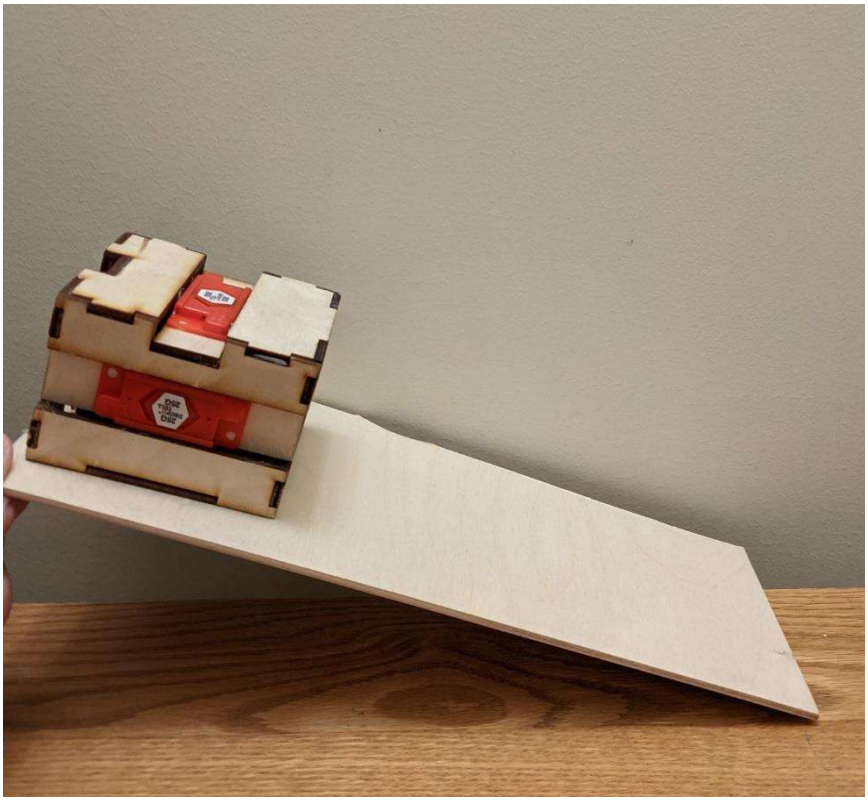

Figure 7.5: Vaccine Vile Package on simulated ramp

7.2.5 Payload Integration Testing

Simple tests were run to simulate the loading of syringes and Vial packages in Missions 2 and 3 respectively. Timing would begin as the team member stepped up to the simulated payload bay and stopped once the payload was integrated and the team member stepped back away from the table. The testing of the syringes was performed assuming they would be provided in a loose pile. Integration of the vial package was to be performed as quickly as possible while also ensuring its sensors were not tripped in the rush to insert it into the deployment mechanism.

7.3 Flight Test Schedule and Flight Plan

Test flights are a critical aspect of testing to ensure proper function of all components once integrated into the aircraft. To ensure time to adjust and fix problems on the aircraft, flight tests will be broken into four days within a week between them as depicted in Table 7.2.

The first round of flight testing will be to validate the function of each main component as well as fine tuning the trim of the aircraft. These flights will be performed without the deployment mechanism and vial package and instead will carry ballast to simulate their weight. Once the aircraft is well trimmed and its handling understood by the pilot, the next round of testing will be performed. These tests will ensure the aircraft's ability to take off within the required distance as well as perform the maneuvers required for the missions. The next set of flight flights will be performed with the deployment mechanism and syringes.

These flights will serve to demonstrate that flight loads will not trip the sensor on the vial package as well as demonstrate the aircraft's ability to taxi and deploy the vial package.

Once all previous test flights are performed and meet design and mission requirements, a simulated competition will be run where all three missions will be performed in sequence as it will during the competition. This will allow the team to perform start to finish testing of integration, flight, landing, and deployment such that any possible problems can be found prior to the competition. Additionally, the team can become accustomed to procedures that will be carried out on competition day.

Table 7.2 Flight Test Planning

Date	Objectuve
Mar 10. 2022	Trim the aircraft
	Determine handling and stability
	Account for pilot feed back to improve flight charachteristics
Mar 17. 2022	Indurance flight testing
	Short take off measurements
	Record lap time
	Ensure structural integrity through manuvering
Mar 24. 2022	Flight with payloads
	Taxi and deploy vaccine vial package
	Ensure flight loads dont trip vial package sensors
Mar 31. 2022	Simulated mission one
	Simulated mission two
	Simulated mission three

7.4 Flight Checklist

To reduce the possibility of failure and keep testing conditions safe, the team adhered to a preflight checklist before each flight as depicted in Table 7.3. The aircraft would only be cleared to fly if every inspection was passed. In the event of one or multiple failed inspections, actions can be taken to fix the problem with another attempt at flight allowed to be taken only after another round of inspection.

Table 7.3: Preflight Checklist

Date		Time			
Structural				**Pass**	**Fail**

Static Test	☐	☐
CG test (leading edge location)	☐	☐
Motor Mount Secured	☐	☐
Servos Secured	☐	☐
Wing Secured	☐	☐
Tail Assembly Secured	☐	☐
Landing Gear Assembly Secured	☐	☐
Payload Secured (mission 2 and 3)	☐	☐
Electronics		
Aircraft Battery Voltage Check	☐	☐
Servo Wires Connection	☐	☐
Controller Battery Voltage Check	☐	☐
Fuse Check	☐	☐
Ground Range Test	☐	☐
Aircraft On/Off Switch Test	☐	☐
Controls		
Left/ Right Aileron	☐	☐
Elevator	☐	☐
Rudder	☐	☐
Flap 1	☐	☐
Flap 2	☐	☐
Deployment (mission 3)	☐	☐
Throttle	☐	☐
Propeller		

Secured	☐	☐
Direction	☐	☐
Additional Comments:		

8 Performance Results

8.1 Subsystem Testing Results

Predictions made during the detailed design section were compared to subsystem test results and flight test results to compare the predicted performance against the actual performance.

8.1.1 Wing Point Load Testing

The sample wing subjected to load was tested to failure with the maximum load recorded. Before the sample spar failed, it was supporting a recorded 61lbF. This is greatly more than the predicted weight of the aircraft

which is predicted to be only 7lbs. As such the design of the wing can be adjusted to lighter weaker materials to trade the excess performance of the wing for less weight. This will be done by swapping major structural beams for balsa instead of pressure treated pine as well as replacing the plywood ribs with balsa.

8.1.2 Fuselage Spar Point Load Testing

The sample fuselage was tested to in the point load machine with the maximum load recorded. Before failing the spar was supporting 65lbF which is well within needed margin to handle flight loads. This weight was less than predicted due to manufacturing faults loading a single plate of the beam causing a premature failure as depicted in Figure 8.1. Steps were taken for the next iteration such that the load is better dispersed along the beam to further increase the factor of safety on the beam.

Figure 8.1: Results from fuselage spar point test loader

8.1.3 Vial Box Testing Results

Drop testing with the Vial package showed that the box cannot fall more than 2.6 inches flat onto a face without tripping a sensor. If the package didn't land flat on a face, instead on an edge or corner, it had a higher chance of not tripping the sensor. As such, the ramp will be designed with guides along the edge of the ramp up until 2 inches above the ground such that the package doesn't fall off and trip its sensor.

Ramp testing demonstrated that the optimal length of the ramp is 14in at an angle of 25 degrees. As such, the landing gear will only need to provide ground clearance of 6 in.

9.0 Bibliography

[1] Sadraey, M. H., “Aircraft Design: A Systems Engineering Approach”, 1st ed., Wiley, Chichester, West Sussex, U.K., 2013.

[2] Hoerner, S.F., “Fluid-Dynamic Drag”, ", 2nd ed., Published by author, 1992.

[3] Anderson Jr., J. D., “Fundamentals of Aerodynamics”, 6th ed., McGraw-Hill Education, Columbus, 2016.

[4] Shevell, R. S., “Fundamentals of Flight”, 2nd ed., Prentice Hall, Englewood Cliffs, N.J., 1989.

[5] Etkin, B., Reid, L.D., “Dynamics of Flight: Stability and Control”, 3rd ed., Wiley, New York, 1995.